

High energy heavy-ion collisions pot pourri

by Uncle Yves

[get the postscript version here](#)

Contents

1 Kinematics	7
1.1 Light-cone variables	7
1.2 Rapidity variables	8
1.3 Pseudo-rapidity variable	8
1.4 Nucleon-nucleon collisions:	9
2 Quarks gluons and other animals	11
2.1 The MIT Bag Model	12
2.2 Deconfinement	12
3 Heavy-ion collision dynamics	13
3.1 Pre-equilibrium phase	16
3.2 Equilibrated phase	17
3.2.1 Thermodynamics variable	17
3.2.2 Energy-momentum tensor	17
3.2.3 Equation of motion	17
3.2.4 Equation of State	18
3.2.5 Initial conditions	20
4 Hard scattering	23
4.1 Definitions	23
4.2 Counting rules	25
4.3 Parton distributions in coordinate and momentum space	26
4.3.1 In vacuum	26
4.3.2 In nuclear medium	26
4.4 Hard processes in heavy-ion collisions	26
4.4.1 Jet quenching	28
4.4.2 Photon tagged jets	34
4.4.3 Photon tagged-jet	34
5 Photons probes of HIC dynamics	43
5.1 Why photons?	43
5.2 Photon sources	44
5.2.1 Photon production during the pre-equilibrium partonic cascade	44
5.2.2 Photon production in the quark gluon plasma: thermal photons	49
5.2.3 Photons emission and collision dynamics	50
5.2.4 High mass di-photons	52
5.2.5 Photon production in the hadronic gas	55
5.2.6 Decay photons	57
5.3 Concluding remark on direct photons	60

5.4	Photon interferometry	63
5.4.1	Photon statistics in quantum optics	63
5.4.2	Application to particle and nuclear physics	63
5.4.3	Photon-photon correlation	67
5.5	Photons and DCC	75
5.6	Photons and heavy mesons	75
5.7	Measuring photons	75
5.7.1	High momenta photons	75
5.7.2	Low momenta photons	76
5.7.3	Extraction of meson spectra	76
5.7.4	Two-photon correlation function	79
5.8	Data and Calculations	81

Introduction

The purpose of heavy-ion physics is to study nuclear matter under extreme conditions from nucleus-nucleus (AA) collisions. At collider energies, colliding nuclei can be viewed as two clouds of valence and sea partons which interact passing through each other. Quantum Chromodynamics predicts that partonic final state interactions produce a new phase of matter, a plasma of quarks and gluons. This new state of matter is a transient rearrangement of the correlations among quarks and gluons contained in the incident baryons into a larger but globally still color neutral system with however remarkable theoretical properties. This plasma expands and becomes cooler and more dilute. In presence of a first-order deconfinement phase transition, the plasma will pass through a mixed phase of quarks, gluons and hadrons, before the hadrons lose thermal contact and stream freely towards the detector. The open questions experiments must answer are to find out what the structure of matter formed in heavy-ion collisions is, and verify if the initial partonic system attains kinetic and/or chemical equilibrium. To achieve equilibrium enough time for formation and equilibration must be available. It is estimated that this time amounts to about 3-5 fm/c at RHIC energies and to more than 10 fm/c at LHC energies.

Relativistic heavy-ion collisions thus provide the experimental information on the fundamental prediction of the Standard Model by searching for the quark-gluon plasma and exploring the physics of this new state of matter. However, it is as important to study at the same time asymmetric systems like proton-nucleus (pA) as well as proton-proton collisions to disentangle the contribution of different physics processes to the same signal.

Chapter 1

Kinematics

Reference [1]

$$\hbar = c = 1$$

1.1 Light-cone variables

- In the reaction:

$$b + a \rightarrow c + X$$

if the detected particle can be identified as originating from one of the colliding particles (a or b), one says that c is **fragmenting** from the projectile b (or the target a).

- Four-momentum:

$$c \equiv (c_0, c_T, c_z) = (c_0, c_x, c_y, c_z)$$

- Forward (backward) light-cone momentum of c :

$$c_{+(-)} = c_0 \pm c_z$$

- Lorentz transformation of $c_{+(-)}$:

$$c'_{+(-)} = \gamma(1 - \beta) c_{+(-)}$$

- Longitudinal-momentum fraction x :

$$x_+ = \frac{c_0 + c_z}{b_0 - b_z} \rightarrow x \text{ at high energies when } c_0 \sim c_z$$

$$0 \leq x \leq 1$$

x is Lorentz invariant.

- Invariant mass of a free particle:

$$c^2 = c_0^2 - \vec{c}^2 = m_c^2$$

- Transverse mass of a free particle:

$$c_0^2 - c_z^2 = m_c^2 + c_T^2 = m_{c_T}^2$$

- Feymann scaling variable:

$$x_F = \frac{c_z^*}{c_z^*(max)} * = CM \text{ quantity}$$

$c_z^*(max)$ is the maximum value of c_z attained in the reaction $b + a \rightarrow c + X$ when X consists of a single particle with a rest mass which corresponds to the minimum value of the rest mass of X allowed by conservation laws (baryon number, charge, etc...).

1.2 Rapidity variables

- Definition:

$$y = \frac{1}{2} \ln \left(\frac{p_0 + p_z}{p_0 - p_z} \right)$$

It is related to the ratio: $\frac{x_+}{x_-}$

- Lorentz transformation:

$$y' = y - \frac{1}{2} \ln \left(\frac{1 + \beta}{1 - \beta} \right)$$

- Relations:

$$\begin{aligned} p_0 &= m_T \cosh y \\ x_+ &= \frac{m_{cT}}{m_b} e^{y-y_b} \quad x_- = \frac{m_{cT}}{m_a} e^{y_a-y} \\ y &= y_b + \ln x_+ + \ln \left(\frac{m_b}{m_{cT}} \right) \quad y = y_a - \ln x_- - \ln \left(\frac{m_a}{m_{cT}} \right) \end{aligned}$$

- Usage:

- to describe particles produced with a momentum close to the beam momentum, use x_+
- to describe particles produced in the central rapidity region ($\frac{y_b+y_a}{2}$) use y

1.3 Pseudo-rapidity variable

To be used when only \vec{p} is measured and not the energy p_0

- Definition:

$$\eta = -\ln \left[\tan \left(\frac{\theta}{2} \right) \right]$$

θ is the angle between \vec{p} and the beam direction.

- Relations:

$$\begin{aligned} \eta &= \frac{1}{2} \ln \left(\frac{|\vec{p}| + p_z}{|\vec{p}| - p_z} \right) \\ |\vec{p}| &= p_T \cosh \eta \\ p_T &= \sqrt{p^2 - p_z^2} \\ p_z &= p_T \sinh \eta \\ \frac{dN}{d\eta dp_T} &= \sqrt{1 - \frac{m^2}{m_T^2 \cosh^2 y}} \frac{dN}{dy dp_T} \end{aligned}$$

1.4 Nucleon-nucleon collisions:

$$3 \text{ GeV} \leq \sqrt{s} \leq 100 \text{ GeV}$$

- Cross-sections:

$$\sigma_{tot} \simeq 40 \text{ mb} = \sigma_{inelastic} + \sigma_{elastic}$$

$$\sigma_{inelastic} \simeq 30 \text{ mb}$$

$$\sigma_{total} = 48 + 0.522 (\ln p)^2 - 4.5 \ln p$$

$$\sigma_{elastic} = 11.9 + 26.9p^{-1.21} + 0.169 (\ln p)^2 - 1.85 \ln p$$

p in GeV/c

- Particle production:

- about half of CM energy, \sqrt{s} , is used to produce particles
- 80-90% of produced particles are pions
- multiplicity:

$$N_{charged} = 0.88 + 0.44 \ln s + 0.118 (\ln s)^2$$

s in GeV^2

$$N_{total} = N_{charged} \frac{3}{2}$$

- particles which resemble the incident particles in the fragmentation regions ($x \sim 1$) are called **leading particles**.
- rapidity distribution:

$$\frac{dN}{dy} = A (1 - x_+)^a (1 - x_-)^a \quad a \sim 3 - 4$$

- invariant cross-section:

$$E \frac{d\sigma}{d^3p} = [(1 - x_+) (1 - x_-)]^4 [110e^{-6.6p_T} + 35e^{-4.2p_T}] \text{ mb}c^3/\text{GeV}^2$$

- m_T scaling:

$$E \frac{d\sigma}{d^3p} = \frac{Ae^{-m_T/T}}{(m_T/\text{GeV})^\lambda}$$

$$\lambda=1.5, T=0.290 \text{ GeV}, A=13.9 \text{ mb GeV}^{-2}c^3$$

- definitions:

- * $p_T \ll 1 \text{ GeV}/c$: soft particles (phenomenological QCD)
- * $p \gg 1 \text{ GeV}/c$: hard particles (perturbative QCD)

Chapter 2

Quarks gluons and other animals

Quarks	Q	I _z	C	S	T	B	Mass (MeV)
u	2/3	1/2	0	0	0	0	5.6±1.1
d	-1/3	-1/2	0	0	0	0	9.9±1.1
c	2/3	0	1	0	0	0	1350±50
s	-1/3	0	0	-1	0	0	199±33
t	2/3	0	0	0	1	0	> 90000
b	-1/3	0	0	0	0	-1	≈ 5000

- mass:
The mass reported in the table is the *current* mass, i.e., the mass of the quark in absence of confinement. When the quark is confined in a hadron, the quark acquires an effective mass called the *constituent* mass. It is typically a few hundred MeV.
- QCD
Quantum Chromodynamic is the field theory which describes the strong interaction. The QCD Lagrangian takes the following form:

$$\mathcal{L}_{\text{QCD}} = -\frac{1}{4} \sum_{\mu, \nu} F_{\mu\nu}^a F^{\mu\nu a} + \sum_{\text{flavors}} \bar{\psi} (\gamma^\mu \partial_\mu - \mathbb{1}_{\text{flavor}}) \psi - \bar{\psi} \hat{A}_\mu \psi$$

with γ^μ the Dirac Gamma matrices, J^μ the 4 current-vector $\hat{A}_\mu(x) = \sum_{i=1}^8 A_i^\mu(x) \lambda_i$, the Colour potential sum of the 8 gluon-potentials, and $F_i^{\mu\nu}$ the Field intensity tensor which transforms as:

$$F_i^{\mu\nu} = \partial_\mu A_\nu^i - \partial_\nu A_\mu^i + g f_{ijk} A_j^\mu A_k^\nu$$

where the last term describes the self coupling of gluons. The physics of QCD can be divided into two regimes. The first one, the domain of asymptotic freedom, corresponds to high momentum transfer and can be treated by perturbative theory. The second one, the domain of confinement, corresponds to small momentum transfer and can be treated within the lattice theory. By asymptotic freedom one means that for increasing momentum transfer, the quarks cross section decreases, in other words the coupling constant is related to the scale

of the momentum transfer:

$$\alpha_s(q^2) = \frac{\alpha_0}{1 + \alpha_0 \frac{(33-2n_f)}{12\pi} \ln\left(\frac{-q^2}{\mu^2}\right)}$$

where α_0 is the coupling constant for the momentum transfer μ and n_f the number of flavors. When the distance scale of the interaction is small, i.e., when one probes the high momentum component of the quarks distribution, the coupling constant is small. Therefore quarks move almost freely inside hadrons. A perturbative treatment in terms of partons is applicable. The above expression can be rewritten in terms of temperature versus critical temperature for the phase transition:

$$\alpha_s(T) = \frac{6\pi}{(33 - 2n_f) \ln\left(\frac{8T}{T_c}\right)}$$

One often uses the strong interaction coupling constant $g = \sqrt{4\pi\alpha_s}$.

2.1 The MIT Bag Model

The bag model provides a useful phenomenological description of quarks being confined inside hadrons. Quarks are treated as massless particles inside a bag of finite dimension. They are infinitely massive outside the bag. Confinement results from the balance of the pressure on the bag walls from the outside and the pressure resulting from the kinetic energy of the quarks inside the bag. The bag pressure constant, B , is related to the equilibrium radius of the bag:

$$B^{1/4} = \left(\frac{6.12}{4\pi}\right)^{1/4} \frac{1}{R}$$

For a baryon radius $R = 0.8$ fm, $B^{1/4} = 206$ MeV.

Inside the bag perturbative QCD applies. The total color charge of the matter inside the bag must be colorless, thus valid hadronic bags can only contain qqq and $q\bar{q}$ states.

2.2 Deconfinement

Under given conditions of temperature and density QCD Lattice theory predicts that hadronic matter undergoes a phase transition toward a plasma of quarks and gluons in which quarks and gluons are deconfined. The predicted temperature at which this phase transition occurs is about 200 MeV.

Chapter 3

Heavy-ion collision dynamics

It is difficult to find a robust theoretical description of relativistic heavy-ion collisions involving the QCD phase transition to predict observables. Theory can thus serve mainly to motivate particular experimental studies and provide overall consistency checks in the interpretation of the data. The heavy-ion collision at collider energies can be viewed as depicted in Figures 3.1 and 3.2.

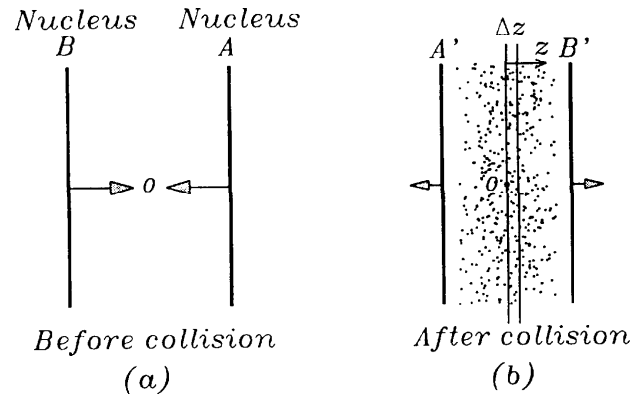


Figure 3.1: *The configuration of two colliding nuclei before collision and after collision with energy deposited in the central region.*

In Bjorken's space-time scenario, which might be the appropriate picture for collisions at $\sqrt{s} \geq 100A$ GeV, the colliding nuclei traverse each other with only little interaction which deposit only part of their kinetic energy to heat up the central rapidity distribution. In the region between the two fast traversing nuclei hot matter is formed with energy densities larger by one or two orders of magnitude than the energy density of normal nuclear matter. Matter in this space-time region is formed of quasi free quarks and gluons and constitutes the pre-equilibrium phase which might lead to a local thermal equilibrium provided that there are enough interactions among partons.

The initial conditions at which the equilibrium is reached are defined by

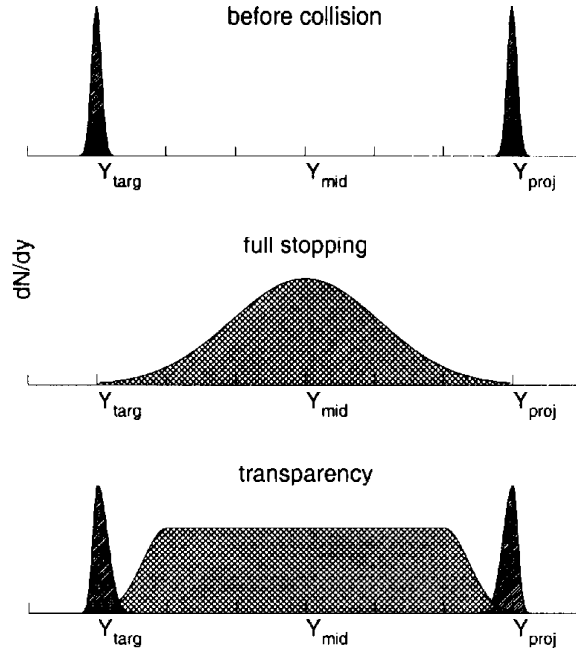


Figure 3.2: *Nuclear stopping scenarios. The particle rapidity distributions are given before the collision and after the collision in the case of a full stopping (Landau) and complete transparency (Bjorken).*

$(z, t) = (0, 0)$ and the proper time τ_0 . The proper time is defined as the local time in the rest frame of any fluid element. For example, if one considers a cylindrically symmetric collisions, the longitudinal proper time is:

$$\tau = \sqrt{t^2 - z^2}$$

Local equilibrium is defined as the coincidence of the exponential slopes of the longitudinal and transverse momentum distributions when they are integrated over a comoving volume with linear dimensions of one partonic mean free path, λ_f . The equilibrium is predicted to be reached after $\tau_0 \approx 0.7\lambda_f$, i.e., $\tau_0 \approx 0.2 - 0.3$ fm/c at collider energies.

After τ_0 the plasma may evolve according the law of hydrodynamics. Chemical equilibration is driven by the two-body reactions $q\bar{q} \leftrightarrow q\bar{q}$ and gluon multiplication and its inverse process, gluon fusion $g\bar{g} \leftrightarrow g\bar{g}$. The hot matter expands, cools down to a critical temperature $T_c = 160$ MeV ($\epsilon_c = 1.45$ GeV/fm³) and the hadronization takes place. The system then enters into a mixed phase where a phase transition occurs. When all of the QGP has converted into hadrons, the gas again expands and cools till freeze-out temperature ($T_f \sim 100$ MeV) is reached. The hadrons finally stream out of the collision region at freeze-out temperature. We shall now review how the various phases considered and depicted in Figure 3.4 can be formalized.

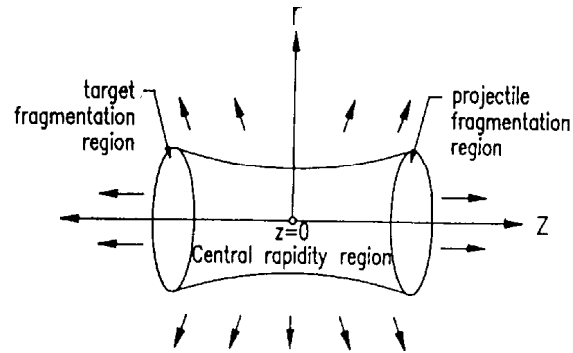


Figure 3.3: Schematic diagram showing the spatial evolution of the matter formed after the central collision of two identical nuclei in the center of mass frame.

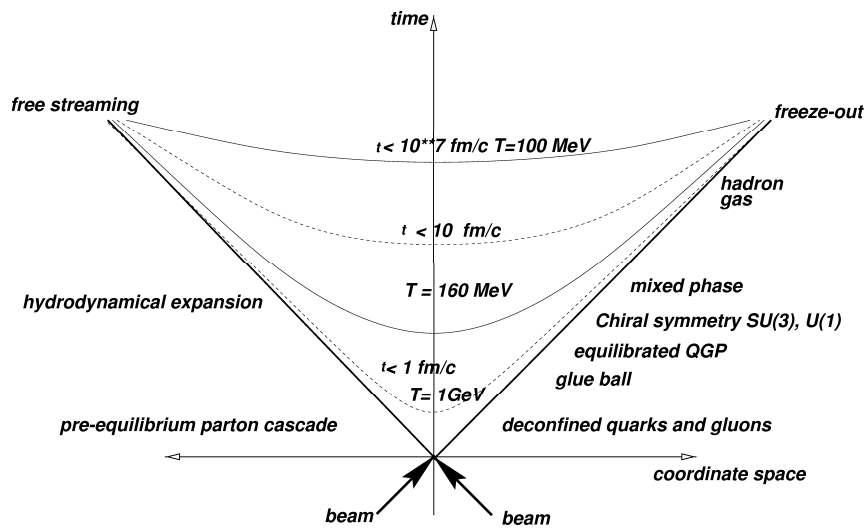


Figure 3.4: Space-time picture of a nucleus-nucleus collision.

3.1 Pre-equilibrium phase

In the pre-equilibrium phase the dynamic of partonic can be described as a cascade of freely colliding partons. This is the approach taken by the Parton Cascade Model [3]. The space-time evolution of the partons distribution is described by a transport equation where the collision term is described by QCD processes calculated within the perturbation theory. The main hypothesis called the factorization hypothesis is that the collisions during the cascade are independent of each other. The initial partons distribution is described by the distribution in phase-space (\vec{p}, \vec{r}) at time $t = t_0$ of parton of type $a \equiv (u, d, \dots : q, \bar{q}, g)$:

$$F_a^0(\vec{p}, \vec{r}, t = t_0) = \sum_{i=1}^N P_a^{N_i}(\vec{p}, \vec{P}, \vec{P}) R_a^{N_i}(\vec{r}, \vec{R}, \vec{R})$$

where $P_a^{N_i}$, and $R_a^{N_i}$ are the momentum and spatial distribution of the parton in the nucleon as a function of the parton momentum (position), the nucleon momentum (position) and nucleus momentum (position). The momentum distribution of partons can be expressed in terms of the transverse momentum distribution parametrized as:

$$g(\vec{p}_\perp) = \frac{1}{\pi\xi^2} \exp\left(\frac{-|\vec{p}_\perp|^2}{\xi^2}\right)$$

and the nucleon structure function $f_a^{N_i}(x, Q_0^2)$ evaluated at fixed transferred momentum $Q_0 \sim 1$ GeV which is experimentally measured by electron scattering for example. On therefore writes:

$$P_a^{N_i}(\vec{p}, \vec{P}, \vec{P}) = \frac{x}{x_{R_a}} f_a^{N_i}(x, Q_0^2) g(\vec{p}_\perp)$$

with the fractional longitudinal momentum of the parton:

$$x = \frac{p_a}{P_{N_i}}$$

$$x_{R_a}^2 = x^2 + \frac{m_{\perp a}^2}{(P_{N_i})^2}$$

with P_{N_i} the nucleon momentum within the nucleus and $m_{\perp a}^2 = p_\perp^2 + m_a^2$.

The evolution of the phase-space distribution of the partons is then described by the relativistic Uehling-Uhlenbeck equation:

$$p^\mu \partial_\mu F_a = \sum_{coll} E_a C$$

where C describes the collision term. This equation follows the evolution of the system until it equilibrates i.e., until partons are isotropically distributed in phase space. An effective local temperature is defined in an elementary volume cell in the center of the system. Its evolution can be parametrized of Au+Au at $\sqrt{s} = 200A$ GeV as:

$$T(\tau) = 950 \text{ MeV} \left(\frac{\tau}{0.05 \text{ fm}/c} \right)^{-0.30}$$

where $\tau = \sqrt{(t - 1 \text{ fm}/c)^2 - z^2}$ represents the proper time, z being the longitudinal coordinate.

3.2 Equilibrated phase

The initial condition at equilibrium can be estimated from a parton cascade calculation. Relativistic hydrodynamics will then be used to describe the expansion of the hot and compressed central region characterized by a constant baryon density and constant energy density.

3.2.1 Thermodynamics variable

The dynamics of the system is described at different space-time points as the system evolves by:

- ϵ : the energy density
- p : the pressure field
- T : the temperature field
- $u^\mu = dx^\mu/d\tau$: the 4-velocity field

The energy density and the pressure at a space-time point are measured in the frame in which the velocity of a fluid element at that point is zero, i.e., $u^\mu = (1, 0, 0, 0)$. The energy density, the pressure and the temperature are related by the EOS:

$$\epsilon = \epsilon(p, T)$$

3.2.2 Energy-momentum tensor

$T^{\mu\nu}$ is defined as the momentum in the μ direction per unit 3-surface area perpendicular to the ν direction. In the frame in which the fluid is at rest:

$$\begin{aligned} T^{*00} &= \epsilon \\ T^{*ij} &= p\delta^{ij} \text{ if the pressure is isotropic} \end{aligned}$$

The energy-momentum tensor in terms of energy density and pressure is:

$$T^{\mu\nu} = (\epsilon + p) u^\mu u^\nu - g^{\mu\nu} p$$

where $g^{\mu\nu}$ is the metric tensor.

3.2.3 Equation of motion

In Bjorken's hydrodynamik model the space-time evolution of the system is described as an one dimensional expansion. It is assumed that a particle produced at $z = t = 0$ propagates freely along a straight trajectory. In the rest system of the produced particles, the fragments propagate along hyperbols of constant longitudinal proper time. The system is approximated as an idealized continuum with a longitudinal translational symmetry so that a Lorentz transformation along the longitudinal direction leads to the same initial conditions and the same dynamics of the system. The dynamics of the system can then be specified by the thermo-dynamical variables as a function of the the proper time (Lorentz invariant quantity):

$$\begin{aligned} \epsilon &= \epsilon(\tau) \\ p &= p(\tau) \\ T &= T(\tau) \end{aligned}$$

and the motion is governed by the hydro-dynamical equation which comes from energy and momentum conservation:

$$\frac{\partial T^{\mu\nu}}{\partial x^\mu} = 0$$

Since it is assumed that the system undergoes a purely longitudinal boost-invariant expansion, the equation of motion reduces to an equation for the thermodynamic variables ϵ and p as:

$$\frac{\partial \epsilon}{\partial \tau} + \frac{(\epsilon + p)}{\tau} = 0$$

This equation implies:

$$\epsilon \tau^{4/3} = \text{Constant} \quad (3.1)$$

3.2.4 Equation of State

Equation of states for the various phases of matter during the collision are defined [4][5]

Quark-gluon plasma

It is described by an ideal gas EOS for massless non-interacting particles:

$$p(\epsilon, \rho_B) = \frac{\epsilon}{3}$$

Two parametrizations are proposed here:

- Sollfrank *et al.* [4]

$$p = \frac{(32 + 21N_f)\pi^2}{180} T^4 + \frac{N_f}{2} \mu_q^2 T^2 + \frac{N_f}{4\pi^2} \mu_q^2 - B$$

$$\epsilon = 3p + 4B$$

$$\rho_B = N_f \mu_q^2 T + \frac{N_f}{\pi^2} \mu_q^3$$

where $\mu_q = \mu_B/3$; B is the bag constant (connected in the MIT bag model with the energy necessary to form a bag out of the QCD vacuum); $N_f = 2.5$ is the number of flavors which simulates effects of the finite strange quark mass.

- Srivastava *et al.* [5]

$$\epsilon = 3P = [a_2 \lambda_g + b_2 (\lambda_q + \lambda_{\bar{q}})] T^4$$

where $a_2 = 8\pi^2/15$, $b_2 = 7\pi^2 N_f/40$, $N_f \approx 2.5$ is the number of dynamical quark flavors, λ_k is the fugacity for the parton species k and is defined by:

$$n_g = \lambda_g \widetilde{n}_g, \quad n_q = \lambda_q \widetilde{n}_q \quad (3.2)$$

where \widetilde{n}_k is the equilibrium density of the parton species k :

$$\widetilde{n}_g = \frac{16}{\pi^2} \zeta(3) T^3 = a_1 T^3 \quad (3.3)$$

$$\widetilde{n}_q = \frac{9}{2\pi^2} \zeta(3) N_f T^3 = b_1 T^3$$

Hadronic phase

It is described by a hadron gas EOS built in the following way:

1. the hadron gas contains the following hadrons with their anti-particles:

$$\pi, K, \eta, \rho, \omega, K^*, p, n, \eta', \phi, \Lambda, \Sigma, \Delta, a_1, \Xi, \Sigma (1385)$$

it does not change too much to only include mesons up to the ω meson.

- (a) in case of a dilute gas, non-interacting hadrons in chemical equilibrium are considered. One starts from the grand canonical partition function:

$$\{\mathcal{Z}^H(T, V, \mu_B, \mu_S) = \prod_h \exp[Z_h(T, V, \mu_h)]\}$$

where V is the volume, the product is taken over the different hadron species h , μ_h is the chemical potential of hadron h ,

$$\mu_h = B_h \mu_B + S_h \mu_S$$

where B_h and S_h are the baryon number and the strangeness of hadron h , Z_h is the partition function for the hadron specie h :

$$\ln Z_h(T, V, \mu_h) = \beta V p_h = \frac{g_h \beta V}{6\pi^2} \int_{m_h}^{\infty} dE \frac{(E^2 - m_h^2)^{3/2}}{e^{\beta(E - \mu_h)} \pm 1}$$

where $\beta = 1/T$, g_h is the degeneracy factor, m_h the mass of the hadron and \pm applies to fermions/bosons.

The thermodynamic variables baryon density, energy density and pressure can then be calculated as:

$$\rho_B(T, \mu_B) = \frac{T}{V} \frac{\partial \ln \mathcal{Z}^H}{\partial \mu_B}$$

$$\epsilon(T, \mu_B) = \frac{1}{V} \frac{\partial \ln \mathcal{Z}^H}{\partial \beta}$$

$$p(T, \mu_B) = T \frac{\partial \ln \mathcal{Z}^H}{\partial V}$$

- (b) In case of a dense gas, one has to add a repulsive interaction between particles. This is done by assuming a mean field potential of the form:

$$\mathcal{V}(\rho_B) = \frac{1}{2} K \rho_B^2$$

where K is the mean field repulsion parameter. The partition function is modified as:

$$\begin{aligned} \mathcal{Z}^{MF} &= \exp \left\{ -\beta V \left[\mathcal{V}(\rho_B) - \rho_B \mathcal{V}'(\rho_B) \right] \right\} \\ &\times \prod \exp \left[Z_h \left(T, V, \mu_B^{eff}, \mu_S \right) \right] \end{aligned}$$

where μ_B^{eff} is the effective baryon chemical potential:

$$\mu_B^{eff} = \mu_B - \mathcal{V}'(\rho_B) = \mu_B - K \rho_B$$

and describes the shift in the particle energy by $K \rho_B$ due to the repulsive interaction.

Mixed phase

The phase boundary is determined by pressure balance:

$$p_{HG} = p_{QGP}$$

between the 2 phases at equilibrium. The mixed phase is described by introducing the volume fraction of the QGP defined as:

$$w(\epsilon, \rho_B) = \frac{V^{QGP}}{V^{HG} + V^{QGP}}$$

3.2.5 Initial conditions

References[4][5]

The production and equilibration is not described within hydrodynamics. The calculation starts from initial conditions which specify the state of the system at proper time τ_0 . The uncertainty in the initial conditions arises from the lack of knowledge about the nuclear stopping power and the time scale for the equilibration.

Within Bjorken's model of the collision the geometry of the initial condition at τ_0 is defined by:

- for central collisions, the system has a cylindrical symmetry around the z direction and the radial velocity is zero:

$$\vec{v}_r(t_0, r) = 0$$

in other words (!):

$$u^\mu(z, t) = \frac{1}{\tau}(t, 0, 0, z)$$

- for $t > t_0$, the longitudinal velocity is related to the longitudinal size:

$$v_z = \frac{z}{t}$$

- The system is invariant under longitudinal Lorentz boost, i.e., the thermodynamic quantities depend only on the longitudinal proper time $\tau = \sqrt{t^2 - z^2}$ which equals the local time in the rest frame of any fluid element.
- There is a constant proportionality between the energy density and the proper time (see Equation 3.1):

$$\frac{\epsilon(t_0, z)}{\epsilon(t_0, 0)} = \left(\frac{t_0}{\sqrt{t_0^2 - z^2}} \right)^{4/3} = \gamma(z)^{4/3}$$

where $\gamma(z) = \left[1 - \left(\frac{z}{t_0} \right)^2 \right]^{-1/2}$ is the relativistic γ factor for the Bjorken expansion velocity $\frac{1}{\tau}(t, 0, 0, z)$.

The initial time and temperature can be calculated following two methods (the two I have heard about) modeling the early partons cascade:

1. The self-screened parton cascade model (SSPC)[5]:
Early hard scattering produce a medium which screens the longer ranged color fields associated with softer interactions. When two heavy nuclei collide at sufficiently high energy, the screening occurs on a length scale where perturbative QCD still applies. This approach yields predictions for the initial conditions of the forming QGP without the need for any *ad hoc* momentum and virtuality cutoff parameters.
2. The Hijing Monte-Carlo model[6]:
It combines multiple hard and semi-hard parton scattering with initial- and final-state radiation with Lund string phenomenology for the accompanying soft non perturbative interactions to describe nuclear interactions.

Table 3.1: *Initial conditions for the hydrodynamical expansion phase in central collision of two gold nuclei at RHIC and LHC energies. From reference [5]*

Energy	τ_0 (fm/c)	T_0 (GeV)	$\lambda_g^{(0)}$ -	$\lambda_q^{(0)}$ -	ϵ_0 (GeV/fm ³)
SSPC					
RHIC	0.25	0.668	0.34	0.064	61.4
LHC	0.25	1.02	0.43	0.082	425
HIJING					
RHIC	0.7	0.55	0.05	0.008	4.0
LHC	0.5	0.82	0.124	0.02	48.6

- In the central rapidity region the number of produced particles can be related to the initial conditions:

$$T_0^3 \tau_0 = \frac{2\pi^4}{45\zeta(3)\pi R^2 4a_Q} \frac{dN}{dy}$$

where $a_Q = \frac{47.5\pi^2}{90}$ if the system is initially in the QGP phase, consisting of massless u , and d , and gluons or $a_Q = \frac{4.6\pi^2}{90}$ if the system is in the hadronic phase, consisting of π, ρ, ω ; and η mesons; R is the initial transverse dimension of the system. The evolution of the particle density with time can be calculated using Equation 3.1. Results are shown for RHIC (Figure 3.5) and LHC (Figure 3.6) energies using the SSPC predictions for the initial conditions. It is interesting to notice that gluons are much more abundant than quarks. As a consequence the production of hadrons with a significant “valence-gluon” component, such as η and η' mesons or glue ball may be enhanced.

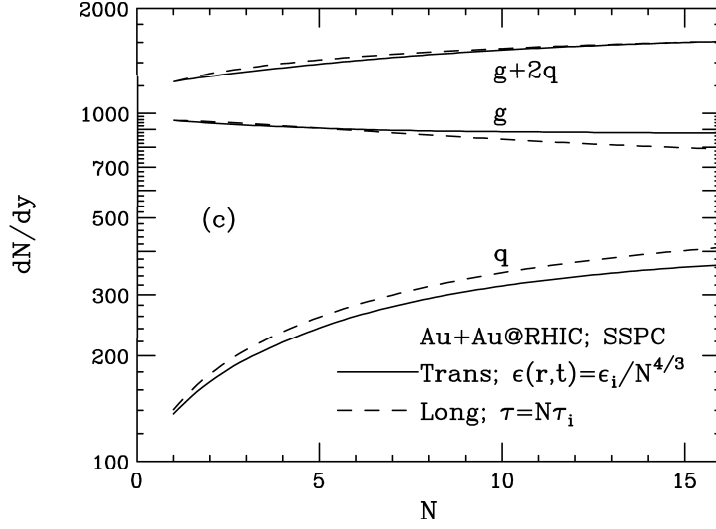


Figure 3.5: Multiplicity of partons with (solid curves) and without (dashed curves) transverse flow at RHIC. From reference [5].

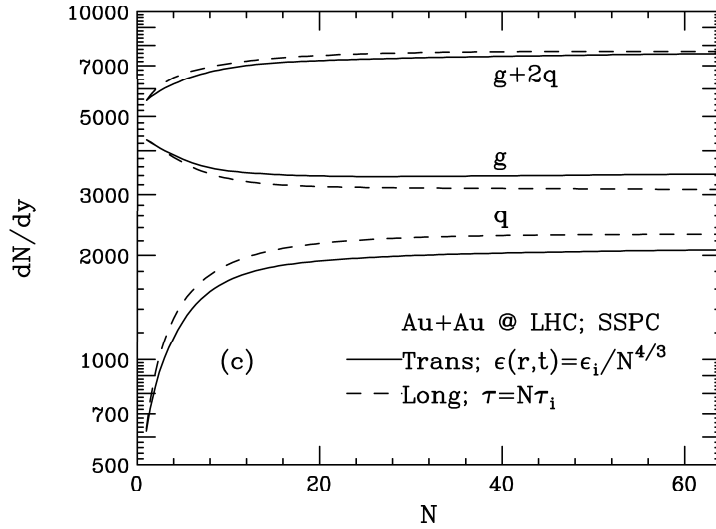


Figure 3.6: Multiplicity of partons with (solid curves) and without (dashed curves) transverse flow at LHC. From reference [5].

Chapter 4

Hard scattering

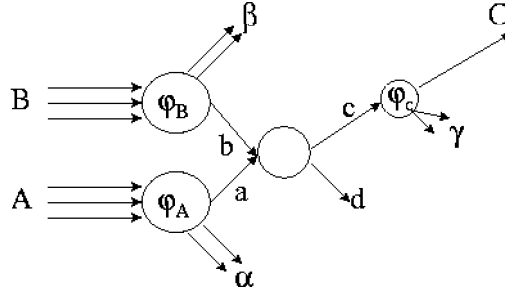
The hard probes associated with hard scattering or hard processes are experimental observables of particular interest because they provide the unique mean to study the partonic structure of hadrons or of extremely hot and dense nuclear matter. In hadron or heavy-ion collisions they are produced in the earliest stage of the collision and their abilities to probe the dense matter are not complicated by the hadronization physics.

4.1 Definitions

Particle and transverse energy production in the central rapidity region of ultra-relativistic heavy-ion collisions can be treated as a combination of perturbative (hard and semi-hard) parton production and non-perturbative (soft) particle production. By *hard processes* one usually means clearly perturbative processes with momentum or mass scales of the order of several tens of GeV. The produced hard parton by fragmentation produces a *jet* which is associated to a parton and is experimentally associated to hadrons clustered in the phase space. Hadronic jets have been observed in $p\bar{p}$ collisions from $p_T \sim 5$ GeV up to $p_T \sim 440$ GeV.

Semi-hard processes refers to QCD-processes where partons with transverse momenta of a few GeV are produced. These partons from semi-hard processes are called *minijets*. The detection of minijets is not possible.

Hard scattering: $A+B \rightarrow C+X$
 A, B : composite particles
 C : detected particle
 a(b): constituent of A(B) called **parton**
 X: $\alpha+\beta+d+\gamma$
 φ : vertex function related with structure function



- Structure function:

$G_{b/B}(x_b, b_T)$ is the probability for finding a constituent of type b in the particle B with a momentum fraction x_b and a transverse momentum b_T :

$$G_{b/B}(x_b, b_T) = \frac{1}{(2\pi)^3} \frac{x_b}{2(1-x_b)} \frac{\varphi_B^2(b)}{(b^2 - m_b^2)^2}$$

where $\varphi_B(b)$ is the vertex function for pulling b out of on B with b off the mass shell; this is not yet calculable within QCD.

- Fragmentation function:

$G_{C/c}(x_C, C_T)$ probability for the parton c to fragment into C with a momentum fraction x_C and a transverse momentum C_T .

- Inclusive cross section:

$$E_C \frac{d^3\sigma}{d^3C} \Big|_{AB \rightarrow CX} = \sum_{ab,cd} \int dx_b db_T dx_a da_T G_{b/B}(x_b, b_T) G_{a/A}(x_a, a_T) \\ \times r(s, s', x_b, x_a) \int dx_C dC_T G_{C/c}(x_C, C_T) E_c \frac{d^3\sigma}{d^3c} \Big|_{ab \rightarrow cd}$$

r is a kinematic factor

$$r = \frac{\lambda'(s', a^2, b^2)}{x_b x_a \lambda(s, A^2, B^2)} \sim 1$$

$$s' = (a+b)^2$$

$$\lambda \sim s \lambda' \sim s'$$

4.2 Counting rules

- In the region $x \sim 1$; $a_T \gg 1\text{GeV}/c$, the interaction of the constituents at very short distance is involved, the corresponding QCD coupling constant becomes small, pQCD can be applicable and the leading behavior of G can be calculated:

$$G_{a/A}(x_a, a_T) \propto (1 - x_a)^{g_a}$$

$$\propto \frac{1}{(a_T^2)^{g_a+1}};$$

with $g_a = 2(N_A - 1) - 1$ is called the counting index and N_A is the number of constituent of on A.

- The elementary cross section can be approximated by:

$$E_C \frac{d^3\sigma}{dC^3} (ba \rightarrow CX') = \frac{1}{(s')^{n-2}} \left[\frac{(X')^2}{s'} \right]^H$$

where H is an empirical parameter, and $X' = (a + b - C)^2 / s'$ the missing mass.

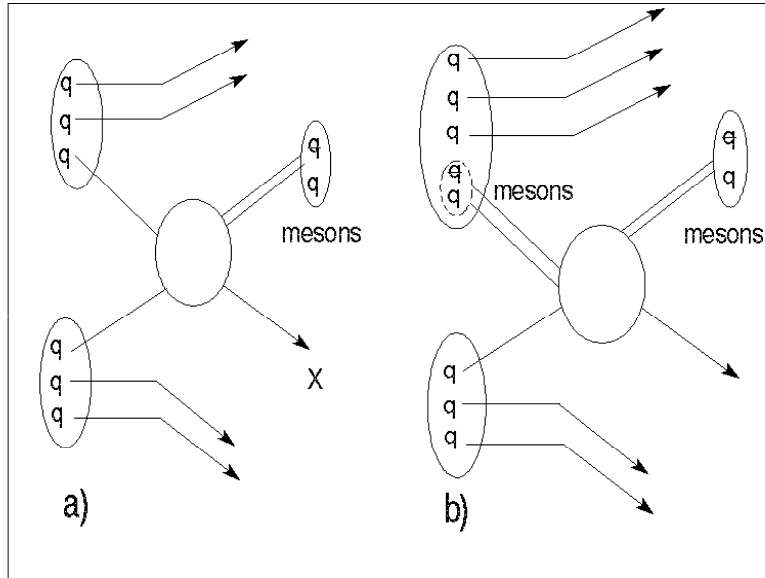
- Thus the rules:

1. N_A is the total number of constituents in A ; N_a the number of constituents in a; $n_s = N_A - N_a$ the number of spectators; $g_a = 2n_s - 1$; idem for g_b ;
2. n is the number of constituent particles participating to the basis process $ba \rightarrow CX$
3. $N = n - 2$; $F = g_a + g_b + 1$

$$E_C \frac{d^3\sigma}{dC^3} \Big|_{AB \rightarrow CX} \propto \frac{(1 - x_r)^F}{(C_T^2)^N}$$

$$\text{with } x_r = \frac{C_0}{\sqrt{s}/2}$$

- Example: $pp \rightarrow \pi X$



elementary process	N_A	N_a	g_a	g_b	F	n	N
$qq \rightarrow qq$	3	1	3	3	7	4	2
$\pi q \rightarrow \pi q$	5	2	5	3	9	6	4

empirically one finds $2N = 8.2$ and $F = 9$ for $pp \rightarrow \pi^+ X$, $\theta_{cm} = 90^\circ$, $x_T > 0.18$, and beam energies from 200 to 400 GeV.

4.3 Parton distributions in coordinate and momentum space

4.3.1 In vacuum

It is deduced from deep-inelastic lepton-nucleon measurements and a functional representation of the parton distribution is usually adopted:

$$xq^a(x, Q) = A_0^a x^{A_1^a} (1-x)^{A_2^a} P^a(x)$$

where a is a flavor label (q, \bar{q}, g); $P^a(x)$ is a smooth function as for example: $1 + \frac{1}{x}$; A_i^a are constants function of Q^2 .

The parton distribution function depends on the momentum scale in which the parton distribution is scaled, therefore the dependence in Q . It is the momentum transfer from the lepton to the constituent and is equal to the four-momentum transfer of the probing intermediate space-like virtual photon.

4.3.2 In nuclear medium

4.4 Hard processes in heavy-ion collisions

The ideal quark-gluon plasma which by definition can be considered as a system of weakly interacting quarks and gluons in both thermal and chemical equilibrium might be difficult to reach in heavy-ion collisions. A generalized quark-gluon plasma which can be defined as an interacting

and deconfined parton system with a large size and a long life-time (several fm/c) might however be reached at RHIC or LHC energies. Hard probes are unique to study the large size and long life-time of the interacting partonic system. They dominate the collision dynamics which will determine the initial conditions of the produced partonic system. Their study will thus enable to probe the early parton dynamics and the evolution of the QGP. Copiously produced at high energies mini-jets are responsible for the thermalization of the hot plasma.

Time scale for producing partons and transverse energy into the central rapidity region by semi-hard collisions is short, typically $\tau \sim 1/p_0 \sim 1$ fm/c where $p_0 \sim 2$ GeV/c is the momentum cut off below which perturbative QCD is not applicable anymore. The soft processes are completed at later times of the collision, $\tau \sim 1/\Lambda_{QCD} \sim 1$ fm/c.

There are two types of hard probes:

1. the thermal emission of photons/di-leptons and charm particles which spectrum can be considered as a thermometer of the dense, thermalized medium constituted of quarks and gluons. The thermal radiation is discussed within the frame of hydrodynamics (see section 3.2 and following).
2. the particle, high p_T particles from jets and J/ψ , suppression by the medium can reveal parton energy loss in dense matter and the deconfinement of the partonic system.

The parton dynamics in the course of a heavy-ion collisions is influenced by various effects during the formation phase as well the thermalized phase effects which could be observed in the hadron transverse momentum spectra resulting from the parton (jet)

fragmentation or in direct photon/dilepton spectra. They are:

- Formation phase (a few tenth fm/c)
 - Initial-state interaction (Cronin effect) between partons and beam nucleons. It results in the smearing of the initial transverse energy of the parton.
 - Nuclear shadowing which describes the depletion of low fractional momentum partons inside the nucleus.
 - The parton cascade which is at the origin of jets and minijets through hard-processes.
 - The soft final-state interaction of produced partons with spectator beam-nucleons. It results in a broadening of the initial transverse energy of the produced parton.
 - The copiously produced minijets lead to the thermalization of the plasma.
- Thermalized QGP phase
 - The earlier produced hard partons by traversing the dense partonic medium loose energy and induces the so-called jet-quenching which can be observed as a suppression of high p_T hadrons resulting from the jet fragmentation. The energy loss proceeds in multiple scattering accompanied by the radiative emission of gluons. The multiple scattering induces a transverse momentum broadening of the jet momentum, Δk_T^2 .

- The weakly interacting thermalized QGP produces a thermal radiation.

The parton then fragments and the QGP hadronizes.

We shall discuss now the second observable often referred to as *jet quenching*.

4.4.1 Jet quenching

The propagation of partons through the dense partonic medium modifies the parton transverse momentum due to induced radiative energy loss (jet quenching) and enhanced acoplanarity and energy imbalance of the two back-to-back jets due to multiple scattering. These effects can be experimentally studied by measuring the energy loss and total transverse momentum broadening squared of partons. They are related to the parton density of the medium that the parton is traveling through.

We shall next discuss the energy loss of partons, traveling through a dense medium, by radiative emission of gluons. The identified jet can contain hadrons both from the fragmentation of the leading parton and from the radiated gluons. Therefore the total energy of the jet is unchanged but the hadrons distribution inside the jet, i.e. the fragmentation function, and the jet profile are modified. To study the jet quenching, one can thus measure the p_T distribution of hadrons inside a jet. However, since the single particle spectrum results from the convolution of jets cross-section and jet fragmentation-function, the high p_T suppression of hadrons will result from quenched jets with a range of initial transverse energies. Therefore can the effect be studied only qualitatively. For a quantitative study one needs to measure photon-tagged jets which momentum is then well defined (see section 4.4.3).

Definitions

A phenomenological model to describe the parton energy through a dense medium is applied. The plasma is formed with a transverse size R_A equal to the size of the colliding nuclei. The parton hadronizes only outside the deconfined phase.

- $D_{h/a}^0(z, Q^2)$: fragmentation function in vacuum for parton a into hadron h at fractional energy $z = E_h/E_a$ and momentum scale Q . It is studied in e^+e^- and $p\bar{p}$ annihilation.
- λ_a is the parton mean free path of the parton inside the plasma. $\lambda_g = 0.5\lambda_q$.
- ϵ_a is the energy loss per scattering.
- $dE_a/dx = \epsilon_a/\lambda_a$ is the energy loss per unit distance. It can be considered independent of the parton energy. It can also be a function of the energy. This energy dependence is not trivial. It can be related to the total transverse momentum broadening Δk_T^2 acquired by the parton through multiple scattering:

$$\frac{dE_a}{dx} = \frac{N_c \alpha_s}{8} \Delta k_T^2 \frac{L}{\lambda_a}$$

where L is the length of the medium, and $N_c = 3$. It is related to the total length the parton has traveled.... the parton knows the history of its propagation.

- $P_a(n, \Delta L)$ is the probability for a parton to scatter n times over a distance ΔL . Assuming a Poisson distribution:

$$P_a(n, \Delta L) = \frac{(\Delta L/\lambda_a)^n}{n!} e^{-\Delta L/\lambda_a}$$

The fragmentation function for the radiated gluon is taken identical to the one of the leading parton. Since its energy ϵ_a is small it also fragments into hadrons with small fractional energy. Finally the parton with initial transverse energy E_T is assumed to travel in the transverse direction of a cylindrical system. Transverse and longitudinal expansions are ignored.

The modified fragmentation function of a parton traveling a distance ΔL is:

$$D_{h/a}(z, Q^2, \Delta L) = \frac{1}{C_N^a} \sum_{n=0}^N \left[P_a(n, \Delta L) \frac{z_n^a}{z} D_{h/a}^0(z_n^a, Q^2) \right] + \langle n_a \rangle \frac{z'_a}{z} D_{h/g}^0(z'_a, Q^2)$$

It is the sum of the fragmentation of the leading parton with reduced energy $E_T - n\epsilon_a$ and the fragmentation of the radiated gluon of energy ϵ_a .

$$z_n^a = \frac{1}{1 - n\epsilon_a/E_T}$$

is the fractional energy after n collisions;

$$z'_a = \frac{z E_T}{\epsilon_a}$$

is the fractional energy of each radiated gluon;

$$N = \frac{E_T}{\epsilon_a}$$

is the number of inelastic scattering limited by energy conservation;

$$C_N^a = \sum_{n=0}^N P_a(n)$$

is a normalization factor. For $N \gg 1$, $\langle n_a \rangle = \Delta L/\lambda_a$ is the average number of scattering within a distance ΔL .

We now need the jets cross-section. Since one wants to compare pp and AA collisions, the two cases are considered:

- pp collision

$$\frac{d\sigma^{pp}}{dy dp_T^2} = K \sum_{abcd,h} \int_{x_{amin}}^1 dx_a \int_{x_{bmin}}^1 dx_b f_{a/p}(x_a, Q^2) f_{b/p}(x_b, Q^2) \frac{D_{h/c}^0(z_c, Q^2)}{\pi z_c} \frac{d\sigma}{d\hat{t}}(ab \rightarrow cd)$$

AA collision

$$\frac{d\sigma^{AA}}{dy dp_T^2} = K \int d^2 r t_A^2(r) \sum_{abcd,h} \int_{x_{amin}}^1 dx_a \int_{x_{bmin}}^1 dx_b f_{a/A}(x_a, Q^2) f_{b/A}(x_b, Q^2) \frac{D_{h/c}(z_c, Q^2, \Delta L)}{\pi z_c} \frac{d\sigma}{d\hat{t}}(ab \rightarrow cd)$$

with the definitions:

$$z_c = \frac{x_T}{2} \left(\frac{e^y}{x_a} + \frac{e^{-y}}{x_b} \right)$$

$$x_{bmin} = \frac{x_a x_T e^{-y}}{2x_a - x_T e^{-y}} \quad x_{amin} = \frac{x_T e^y}{2 - x_T e^{-y}}$$

$$x_T = \frac{2p_T}{\sqrt{s}}$$

The nuclear thickness function is normalized to $A = \int d^2 r t_A^2(r)$. K is a factor to take into account next to leader-order terms and is taken equal to 2.

The structure function of the partons inside the nucleus is derived from the the structure functions of partons in vacuum:

$$f_{a/A} = S_{a/A}(x, r) \left[\frac{Z}{A} f_{a/p}(x, Q^2) + \left(1 - \frac{Z}{A}\right) f_{a/n}(x, Q^2) \right]$$

where $S_{a/A}(x, r)$ is the nuclear shadowing factor.

To study the effective suppression factors one builds the ratio of hadron spectra measure in pp and AA collisions properly normalized by the effective total number of binary NN collisions in a central AA collision:

$$R_{AA}(p_T) = \frac{dN_{AA}/dy/d^2 p_T}{dN_{pp}/dy/d^2 p_T} \frac{1}{\sigma_{in}^{pp} T_{AA}(0)}$$

where $T_{AA}(0)$ is the overlap function of central collisions and is equal to $qA^2/8\pi R_A^2$, $R_A = 1.2A^{1/3}$ fm.

The calculated suppression factor (Figure 4.1) indicates a rise in the region where hard processes are the dominant mechanism for the production of hadrons ($p_T > 5$ GeV/c). This is explained by the fact that the most energetic hadrons originate from the most energetic jets for which the total energy loss is only a small fraction of the initial energy. The suppression is therefore least. This effect will be less important if one assumes the energy-dependent energy loss. The suppression will remain stronger at high momenta. At lower transverse momenta, soft processes play the dominant role. One notices also a dependence with the mean-free path and the energy loss per unit distance. The two quantities are however linked and cannot be extracted separately in a model independent way. Another way is to compare the direct photons with the decay photons from π^0 . High p_T pions will be suppressed because of jet quenching while the photon spectrum will not be affected by the parton energy loss since the electromagnetic interaction between the produced photon and the QCD medium can be neglected. A change in the γ/π^0 at large transverse momentum can also be an indication of parton energy loss (Figure 4.2).

To study the consequence of a parton energy loss with the distance L it travels one can either vary the impact parameter of the size of the colliding nuclei and measure the dependence of the energy loss at a fixed transverse momentum (Figure 4.3). This could provide the mean to study the energy loss dependence with the size of the plasma.

Strategy for studying the parton dynamics:

- Compare the fragmentation function of jets in pp and pA or peripheral AA collisions to study the transverse momentum smearing (beam parton scattering with other beam partons) and transverse momentum broadening (multiple scattering of leading parton with beam partons).

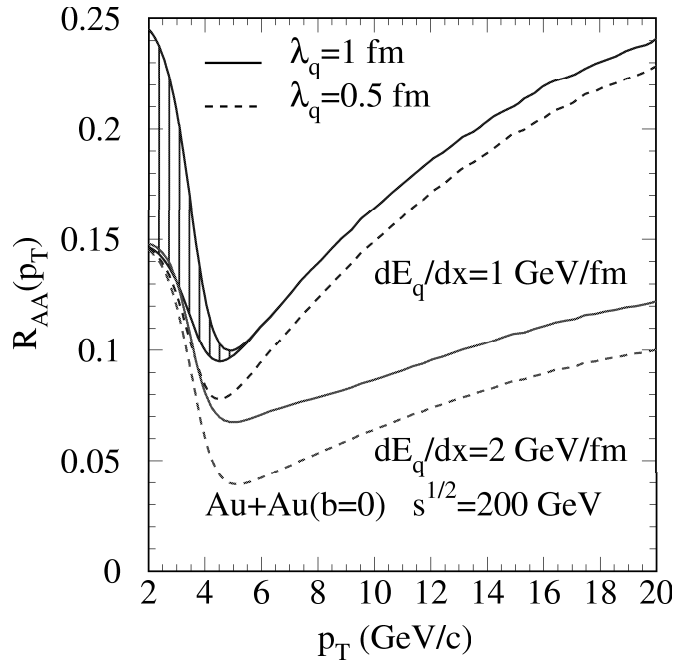


Figure 4.1: The suppression factor or ratio of charged particle p_T spectrum in central Au+Au over that of pp collisions at $\sqrt{s} = 200$ GeV, normalized to the total binary nucleon-nucleon collisions in central Au+Au collisions, with different values of the energy loss dE_q/dx and the mean-free path λ_q of a quark inside the dense medium. From reference [7]

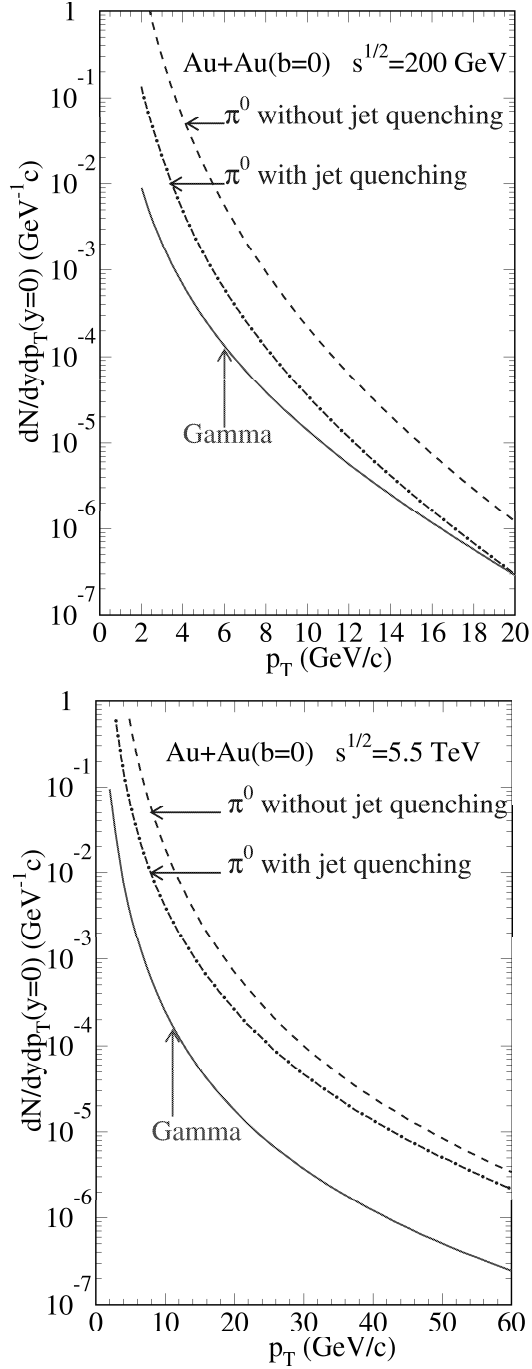


Figure 4.2: The inclusive p_T distribution for π^0 with (solid) and without (dashed) parton energy loss as compared to that of direct photons (dot-dashed) in central Au+Au collisions at $\sqrt{s} = 200 \text{ GeV}$ and $\sqrt{s} = 5.5 \text{ TeV}$. From reference [7].

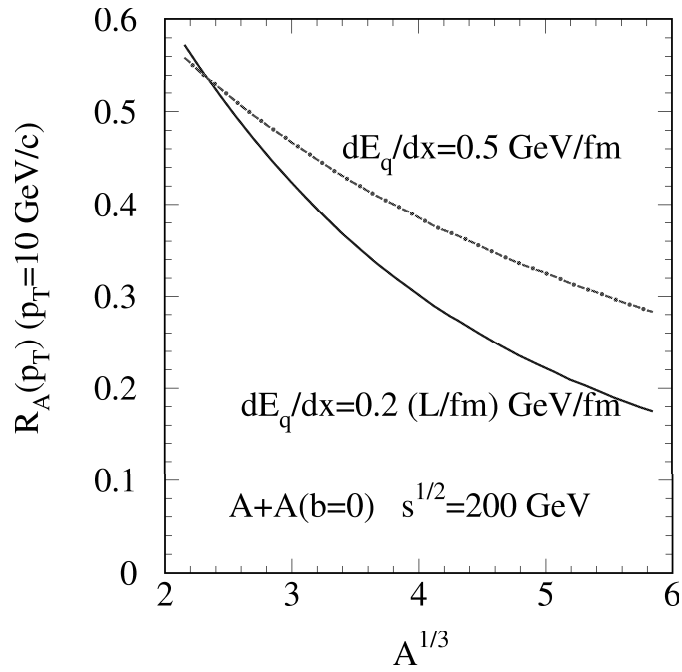


Figure 4.3: The suppression factor for central A+A collisions at $p_T = 10 \text{ GeV}/c$ as a function of the system size for a constant energy loss per unit distance length (dot-dashed line) and an energy loss which increases linearly with the length (solid line). From reference [7].

- Compare pp and central AA to study the energy loss of partons traveling through the dense partonic medium and the momentum broadening in direction transverse to the parton propagation, or k_T^2 broadening.

4.4.2 Photon tagged jets

4.4.3 Photon tagged-jet

In the previous section we have discussed how the energy loss of partons traversing a dense partonic medium can be qualitatively studied from the observation of high p_T hadrons suppression. The difficulty in the interpretation of this kind of observation is that the energy of the parton at the origin of the hadrons in question is not known so that the jet fragmentation can only be studied at an average fractional energy. To overcome this difficulty of not knowing precisely enough the jet energy one can use direct photons to tag the energy of jets which always accompany the direct photons.

We consider than one measures a photon with transverse energy E_T^γ in the rapidity range $\Delta y = 1$ around central rapidity and at azimuthal angle $\phi_\gamma, \overline{\phi}_\gamma = \phi_\gamma - \pi$. We will calculate the p_T distribution of hadrons from the associated jet fragmentation over the kinematical region $(\Delta y, \Delta\phi) = (|y| \leq \Delta y/2, |\phi_\gamma - \overline{\phi}_\gamma| \leq \Delta\phi/2)$. As in the previous section we shall compare pp and AA collisions.

- pp collisions: the multiplicity of hadrons associated with a direct photon is defined as:

$$\frac{dN^{h/\gamma}}{dy dp_T^2} = \frac{1}{dy d^2 p_T} \left(\frac{d\sigma^{h/\gamma}}{dy_\gamma dE_T^\gamma} \Big/ \frac{d\sigma^\gamma}{dy_\gamma dE_T^\gamma} \right)$$

The hadron cross section is obtained by summing over all jets a and hadron species h the cross section for the production of photon-jet event. Using the notations of the previous section:

$$\begin{aligned} \frac{1}{dy d^2 p_T} \frac{d\sigma^{h/\gamma}}{dy_\gamma dE_T^\gamma} &= \sum_{a,h} \int dE_T^a dy_a d\phi_a \\ &\times \frac{d\sigma^{a/\gamma}}{dy_\gamma dE_T^\gamma dE_T^a dy_a d\phi_a} \frac{D_{h/a}^0(p_T/E_T^a)}{p_T E_T^a} \\ &\times \int_{(\Delta y, \Delta\phi)} \frac{dy}{\Delta y} \frac{d\phi}{\Delta\phi} f_0(y_a - y,) \end{aligned}$$

where f_0 is the normalized hadron intrinsic profile around the parton axis (y_a, ϕ_a) . This cross section is modified by initial-state interactions which cause an imbalance between photon and jet transverse momentum and by final-state interactions which change the the jet profile. For that a E_T smearing function (Figure 4.4) and a parton correlation function (Figure 4.5) are defined:

$$g(E_T^a, E_T^\gamma) f_{jet}(y_a, \phi_a) = \frac{1}{d\sigma^\gamma / dy_\gamma dE_T^\gamma} \frac{d\sigma^{a/\gamma}}{dy_\gamma dE_T^\gamma dy_a dE_T^a d\phi_a}$$

which says that for a given photon with a well defined energy more than one jet can be associated because of the E_T^a smearing due to

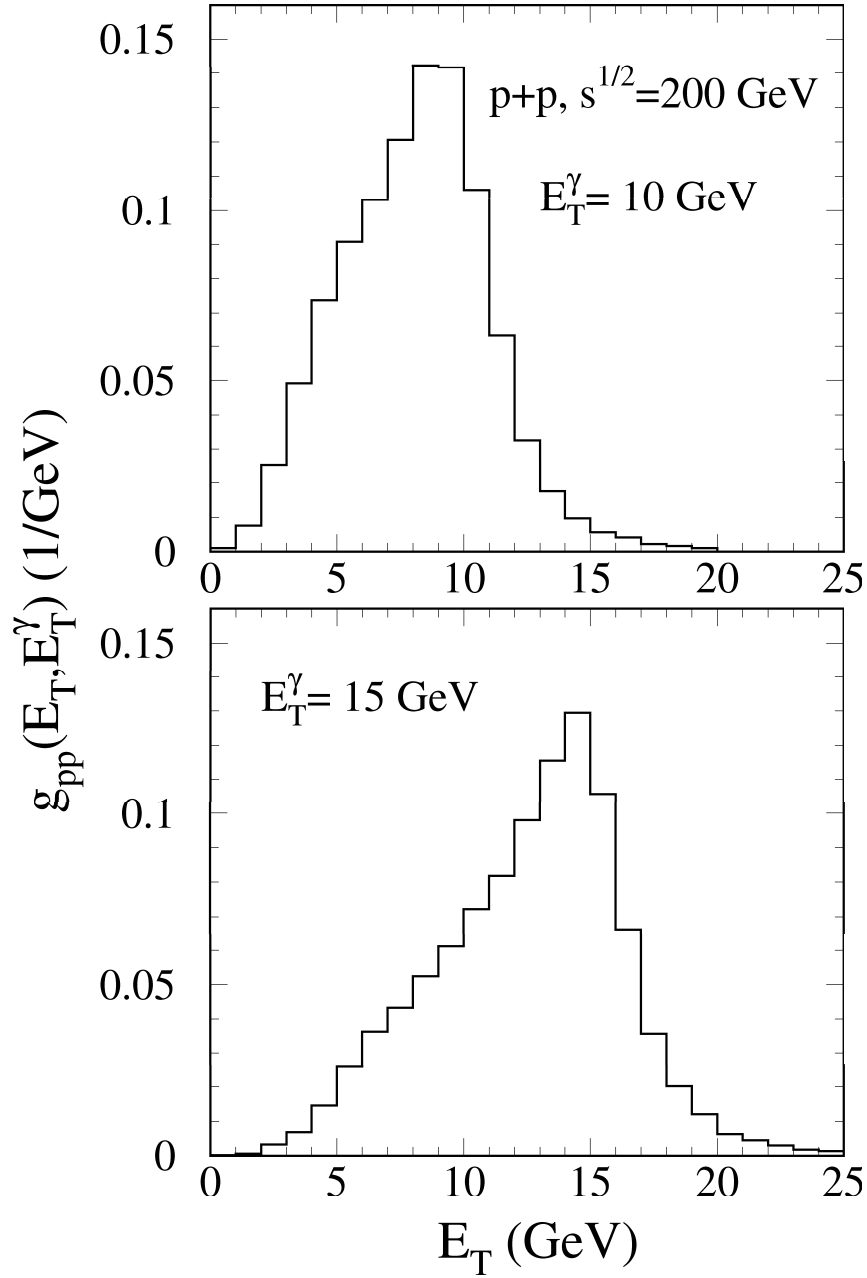


Figure 4.4: The E_T smearing function for the photon-tagged parton jets with $E_T^\gamma = 10, 15 \text{ GeV}$, from HIJING simulations of pp collisions at $\sqrt{s} = 200 \text{ GeV}$. The parton mean energy drops to 8 and 12.6 GeV. From reference [8].

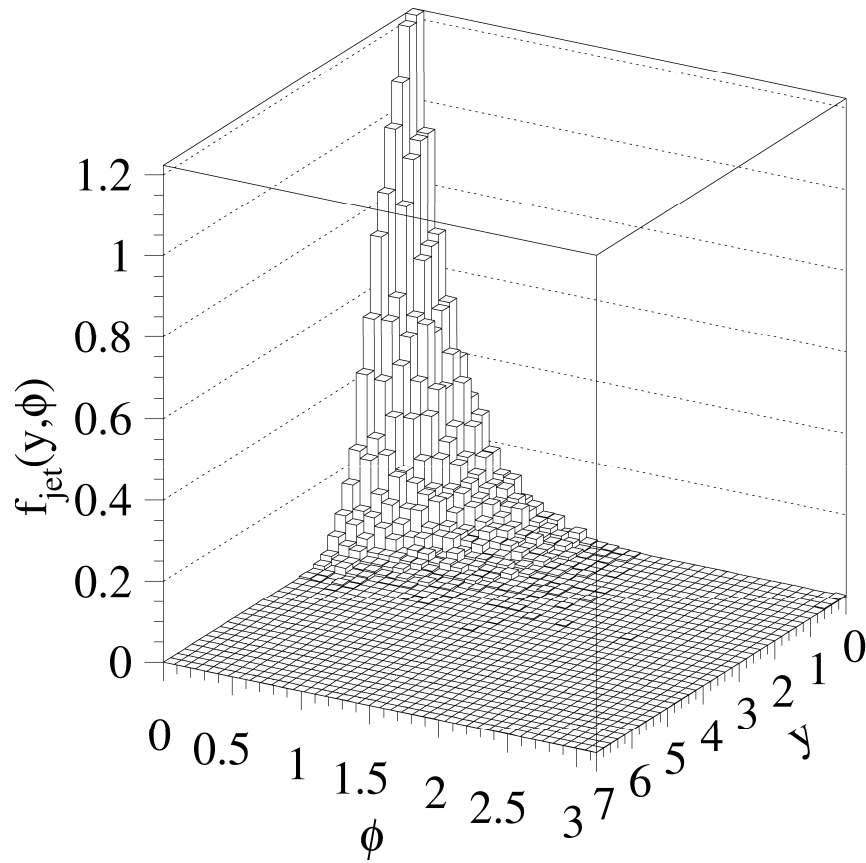


Figure 4.5: The normalized parton correlation from HIJING simulations in rapidity y and azimuthal angle ϕ with respect to the opposite direction of a tagged photon with $E_T^\gamma = 10$ GeV in pp collisions at $\sqrt{s} = 200$ GeV. From reference [8].

initial-state interactions. The hadron multiplicity distribution can thus be rewritten:

$$\frac{dN_{h/\gamma}}{dyd^2p_T} = \sum_{a,h} r_a(E_T^\gamma) \int dE_T g(E_T, E_T^\gamma) \\ \times \frac{D_{h/a}^0(p_T/E_T) C(\Delta y, \Delta\phi)}{p_T E_T \Delta y \Delta\phi}$$

where

$$C(\Delta y, \Delta\phi) = \int_{|y| \leq \Delta y/2} dy \int_{|\phi_\gamma - \bar{\phi}_\gamma| \leq \Delta\phi/2} d\phi f(y, \phi_\gamma - \bar{\phi}_\gamma)$$

can be considered as an acceptance factor for finding the jet fragments in the given kinematical range. For $(\Delta y = 1, \Delta\phi = 2)$, $C(\Delta y, \Delta\phi) = 0.5$. The jet profile is defined as the convolution of the parton correlation function and the hadron intrinsic profile:

$$f(y, \phi) = \int dy_a d\phi_a f_{jet}(y_a, \phi_a) f_0(y_a - y, \phi_a - \phi)$$

The fractional production cross-section of an a -type jet associated with the direct photon is:

$$r_a(E_T^\gamma) = \frac{d\sigma_{a/\gamma}/dy_\gamma dE_T^\gamma}{d\sigma_\gamma/dy_\gamma dE_T^\gamma}$$

and the cross-section for the production of a parton a associated with the photon is:

$$\frac{d\sigma_{a/\gamma}}{dy_\gamma dE_T^\gamma} = \sum_{bc} \int_{x_{bmin}}^1 dx_b f_{b/p}(x_b) f_{c/p}(x_c) \\ \times \frac{2}{\pi} \frac{x_b x_c}{2x_b - x_T e^{y_\gamma}} \frac{d\sigma}{dt}(bc \rightarrow \gamma a)$$

with the notations defined in the previous section. The inclusive fragmentation function associated with the direct photon is:

$$D_{pp}^\gamma(z) = \sum_{a,h} r_a(E_T^\gamma) \int dE_T g(E_T, E_T^\gamma) \frac{E_T^\gamma}{E_T} D_{h/a}^0\left(z \frac{E_T^\gamma}{E_T}\right)$$

with $z = p_T/E_T$ is the hadron momentum as a fraction of the direct photon transverse energy. Finally:

$$\frac{dN_{h/\gamma}}{dyd^2p_T} = \frac{D_{pp}^\gamma(p_T/E_T^\gamma) C(\Delta y, \Delta\phi)}{p_T E_T^\gamma \Delta y \Delta\phi}$$

- **AA collisions:** one uses the impact-parameter average parton distribution per nucleon in a nucleus as in the previous section. The modified fragmentation function reads:

$$D_{AA}^\gamma(z) = \int \frac{d^2 r t_A^2(r)}{T_{AA}(0)} \sum_{a,h} r_a(E_T^\gamma) \int dE_T g_{AA}(E_T, E_T^\gamma) \frac{E_T^\gamma}{E_T} D_{h/a}\left(z \frac{E_T^\gamma}{E_T}, L\right)$$

To measure the modification in the inclusive fragmentation function between pp and AA collisions one follows the steps:

1. select events with a direct photon of energy E_T^γ ; to make sure that the average number of jets with $E_T = E_T^\gamma$ in each central collision is less than 1 one needs to trigger with photons of energy

$$E_T^\gamma \geq E_{Tmin}^\gamma \quad T_{AA}(0) \frac{d\sigma_{jet}}{dydE_T}(E_{Tmin}^\gamma) = 1 \text{ GeV}^{-1}$$

$$E_{Tmin}^\gamma = 40 \text{ GeV at LHC energies.}$$

2. measure the particle spectrum in the kinematical region $(\Delta y, \Delta\phi)$ in the opposite direction of the tagged photon;
3. subtract the background obtained from ordinary events (Figure 4.6);
4. from pp data extract the inclusive jet fragmentation function D_{pp}^γ and from AA D_{AA}^γ ;
5. make the ratio of the two fragmentation functions (one can also compare central and peripheral AA collisions (Figure 4.7);
6. study the modification due to parton energy loss (Figure 4.8). At $z \sim 1$ the remaining contribution comes from the partons which escape the system without any scattering ($n = 0$). This contribution is a measure of the mean-free path of partons:

$$P_a(0) = e^{-L/\lambda_a}$$

At intermediate z the suppression is controlled by the total energy loss:

$$\langle \Delta E_T \rangle = \langle n_a \rangle \epsilon_a = L \frac{dE_a}{dx}$$

and provides a measure of the partons energy loss for fixed E_T and L .

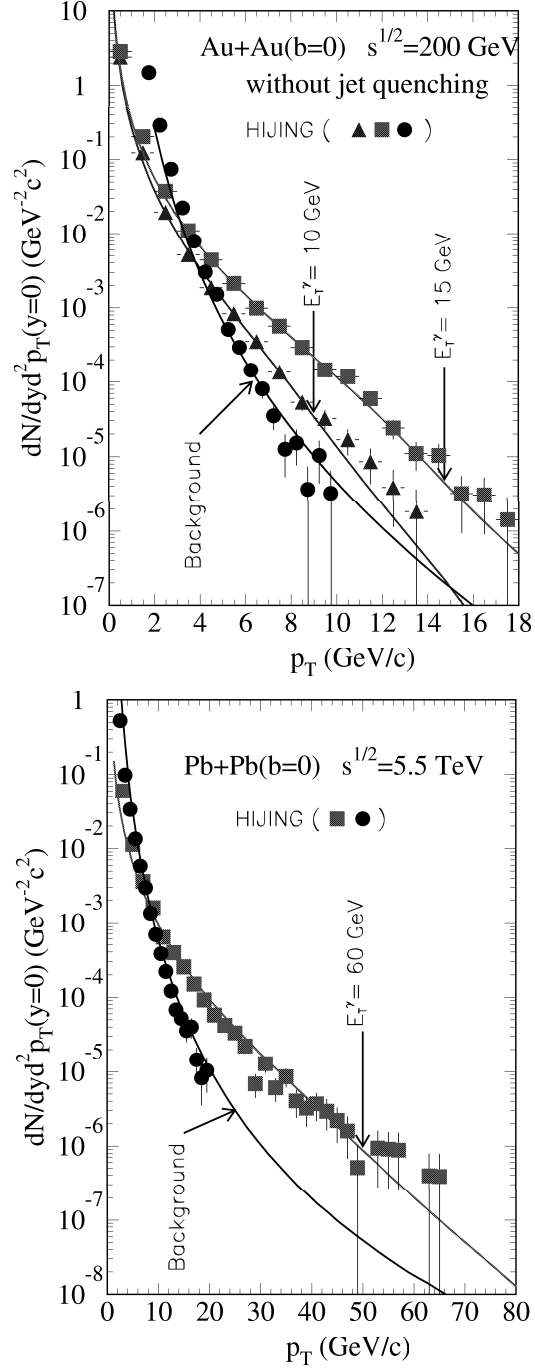


Figure 4.6: *The differential p_T spectrum of charged particles from the fragmentation function of a photon-tagged jet with $E_T^j = 60$ GeV and the underlying background in central Au+Au collisions at $\sqrt{s} = 200$ GeV and $\sqrt{s} = 5.5$ TeV. From reference [8].*

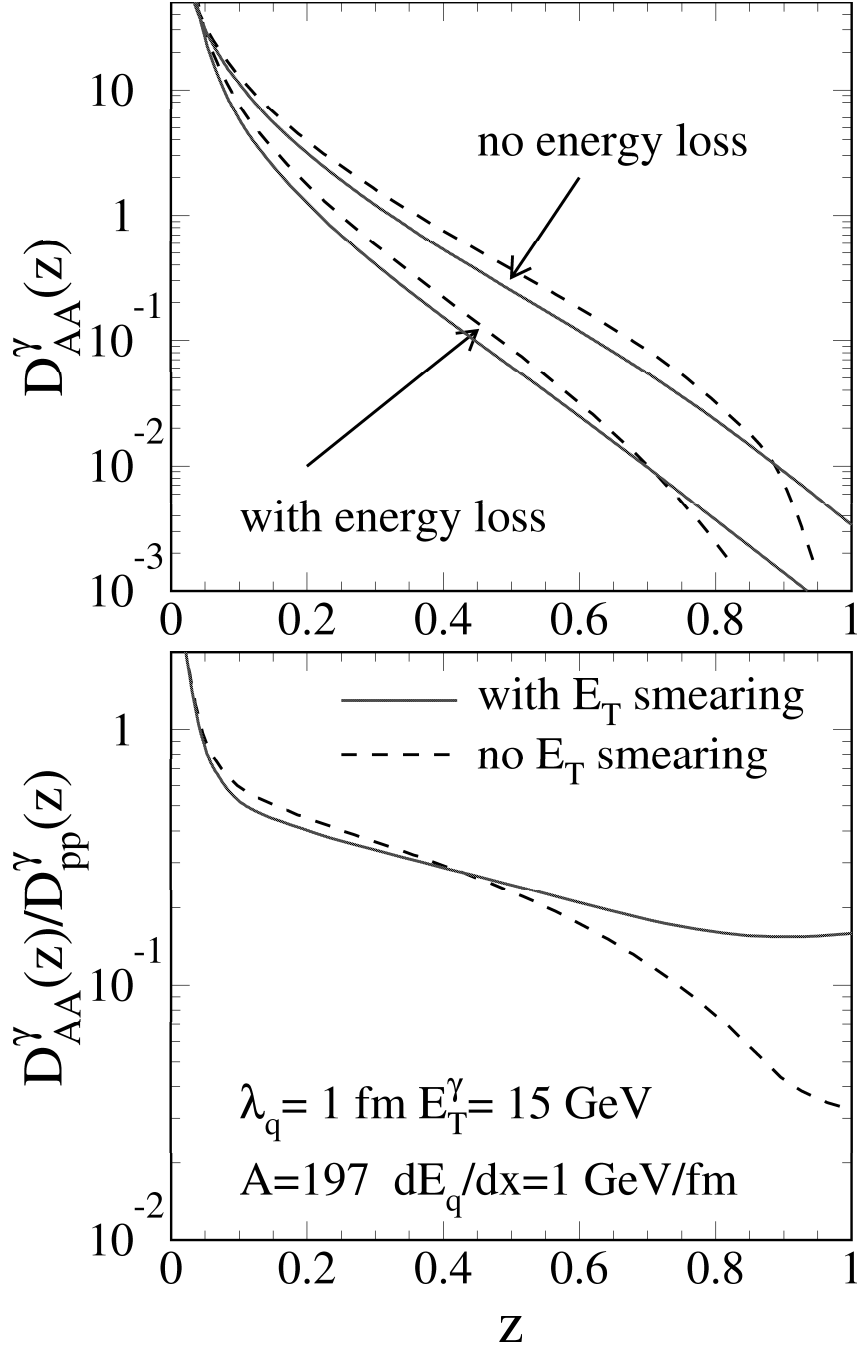


Figure 4.7: Upper panel: The inclusive fragmentation functions with (solid line) and without (dashed line) E_T smearing with and without energy loss. Lower panel: The ratios of the inclusive fragmentation functions from pp and AA collisions. The triggered photon has $E_T^{\gamma} = 15 \text{ GeV}$ in central $\text{Au}+\text{Au}$ collisions at $\sqrt{s} = 200 \text{ GeV}$. From reference [8].

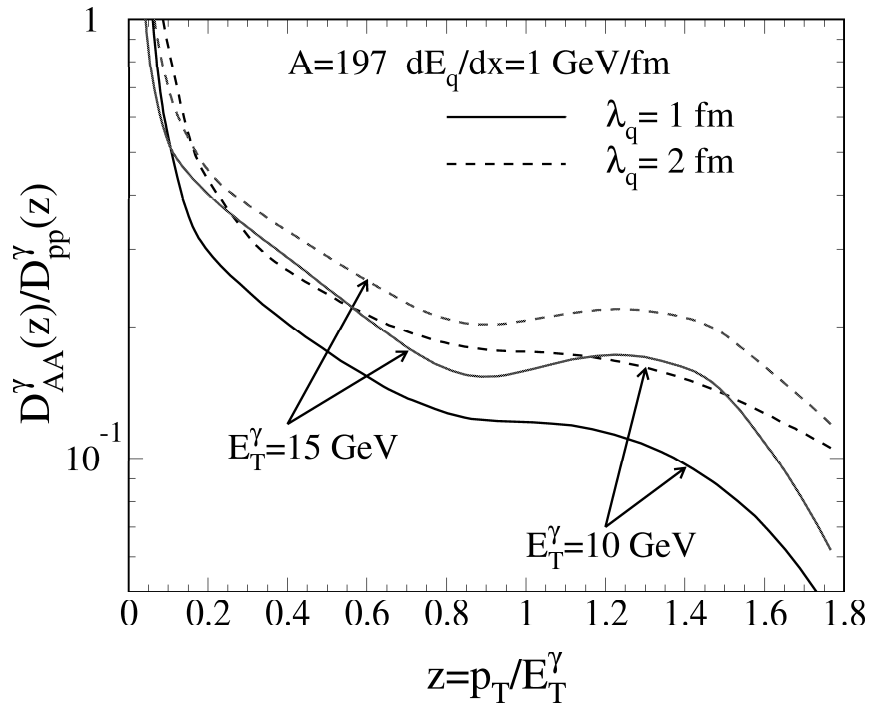


Figure 4.8: The modification factors for the inclusive fragmentation function of photon-tagged jets at given $z=0.4$ as functions of $A^{1/3}$ in central Au+Au collisions at $\sqrt{s} = 200$ GeV. The solid lines are for a distance-dependent parton energy loss, while the dashed lines are for constant energy loss. From reference [8].

Chapter 5

Photons probes of HIC dynamics

Photons have remained one of the most effective probes of every kind of terrestrial or celestial matter over the ages. The main reason for this lays in the fact that photons carry unscathed information about the circumstances of their birth. In a heavy-ion collisions too photons represent a particularly interesting probe of the history of hard and dense nuclear matter.

5.1 Why photons?

- Photons are electro-magnetically interacting particles, therefore is the mean free path of photons traveling through the nuclear medium expected to be quite large and the photons may not suffer a collision after it is produced even in the densest matter. Thus do photons escape from the system without re-scattering.
- The photon production rate and the photon momentum distribution depend on the momentum distribution of the quarks, anti-quarks and gluons in the plasma or of the hadrons in hadronic matter, which are governed by the thermo-dynamical condition of the matter.
- Photons are emitted at all stages of the heavy-ion collision.

Hence, photons convey information on the thermo-dynamical state of the medium at the moment of their production. The hardest photons which accompany the parton cascade evolution during the early stage of the heavy-ion collision shed light on the formation of a partonic matter which at turn radiates a typical softer photon spectrum where from information on thermo-dynamical state of the thermalized plasma can be extracted.

At variance hadrons are not produced until late in the collision when the energy density is lower and their final spectrum is influenced by their last scattering. Since hadrons interact throughout the dense phase of the collision, the hadronic spectra are chiefly determined from the conditions at the freeze-out of matter.

To arrive at definite conclusions about the reaction dynamics and the Equation-Of-state, both of these signals must however be addressed concurrently.

Di-leptons are also an electromagnetic probe and share with photons similar interests. They are however produced with reduced cross-sections as compared to the photon cross-sections by a factor $\alpha = \frac{e^2}{4\pi} = \frac{1}{137}$. On the other hand they carry an additional degree of freedom, the mass. Since the mass is invariant under Lorentz transformation the di-lepton, as well as di-photon, mass spectra are not affected by the transverse flow in the expanding plasma. Photons are because of the Doppler effect.

Both probes convey complementary information and it will be rewarding to compare their spectra. Indeed, photons are mainly produced through gluons Compton scattering and di-leptons through quark-antiquark annihilation, the two probes taken together hence provide valuable tools for probing the early stages of partonic matter, namely the gluon versus the quark content.

5.2 Photon sources

Real photons are produced in all stages of relativistic heavy-ion interactions:

- the initial stage, through hard scattering processes;
- the thermalization phase (if any) of quarks and gluons;
- the phase transition leading to the hadronization phase;
- the hadronic phase;
- the freeze-out phase through final-state interactions and hadron decays.

Therefore photons can tell in principle the entire history of the collision. We shall call *direct* photons all those not coming from final state meson decay.

The photon spectrum as it will be measured during a heavy-ion collision experiment can be calculated by integrating the photon production rate over the space-time evolution of matter and therefore over the thermal and chemical history of the system:

$$E_\gamma \frac{dN}{d^3k} = \int d^4x E_\gamma \frac{dN}{d^4x d^3k} (T(x), u^\mu(x), \lambda_i(x))$$

where $T(x)$ describes the temperature field, $u^\mu(x)$, the 4-velocity field and λ_i the fugacity of the constituent particles. The time evolution of these quantities is described by models as discussed in Chapter 3 and by considering the various phases: pre-equilibrium partonic cascade, equilibrated quark-gluon plasma, mixed parton and hadron gases, and hadron gas.

5.2.1 Photon production during the pre-equilibrium partonic cascade

Photons can be emitted by the initial state collision between constituents of colliding particles with momenta transfer of the order of 1 to 3 GeV. The hard scattering model applies. The basic processes are quark-antiquark annihilation and the gluon scattering, governed by the quark and gluon structure functions and the nuclear shadowing:

Elementary processes[9]

1. Compton scattering:

$$\begin{aligned} g + q &\rightarrow \gamma + q \\ g + \bar{q} &\rightarrow \gamma + \bar{q} \end{aligned}$$

This process is the dominant one. The photon production rate through this process is:

$$\frac{E_\gamma dN_\gamma}{d^3 p_\gamma d^4 x} = \frac{2\alpha_e \alpha_s}{\pi^4} \lambda_q \lambda_g T^2 e_q^2 f_q(p_\gamma) \ln \left(\frac{4E_\gamma T}{k_c^2} + \frac{1}{2} - C \right) \quad (5.1)$$

where $d^4 x$ is the space-time volume element, $C = 0.577721\dots$ is the Euler-Mascheroni constant, e_q the quark charge and k_c is a parameter related to the thermal mass of quarks in the medium, $\alpha_e = \frac{e^2}{4\pi}$ is the electromagnetic fine structure constant, $\alpha_s = \frac{g}{4\pi}$ with g the strong interaction coupling constant, and λ_k the fugacity of parton species k . The function $f_q(\vec{p}_\gamma)$ describes the quark/gluon momentum distribution evaluated at the photon momentum \vec{p}_γ , i.e., the nuclear quark structure function.

2. Quarks annihilation:

$$\begin{aligned} q + \bar{q} &\rightarrow \gamma + g \\ q + \bar{q} &\rightarrow \gamma\gamma \end{aligned}$$

$q + \bar{q} \rightarrow \gamma$ is not allowed by the law of energy-momentum conservation; $q + \bar{q} \rightarrow \gamma\gamma$ is often neglected because its cross section is suppressed by a factor $\frac{\alpha_e}{\alpha_s}$. The photon production rate through this process is:

$$\frac{E_\gamma dN_\gamma}{d^3 p_\gamma d^4 x} = \frac{2\alpha_e \alpha_s}{\pi^4} \lambda_q \lambda_{\bar{q}} T^2 e_q^2 f_q(p_\gamma) \ln \left(\frac{4E_\gamma T}{k_c^2} - 1 - C \right) \quad (5.2)$$

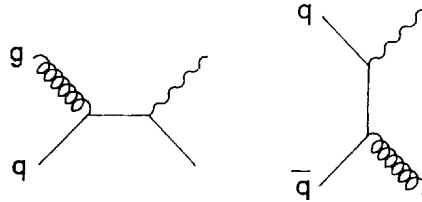


Figure 5.1: Feynman diagrams for $\alpha_s \alpha$ processes (Compton and annihilation graphs) for emission of photons from a quark-gluon system.

The photon distribution from parton collisions is proportional to the initial constituents distribution, i.e., the structure function of quarks and gluons in a nucleon:

$$f(p_\gamma) \propto x_\gamma^{A_1^q} (1 - x_\gamma)^{A_2^q}$$

where $x_\gamma = \frac{E_\gamma^*}{\sqrt{s}/2}$ is the photon light cone variable, and

$$f(p_\gamma) \propto \left(\frac{2E_\gamma^*}{\sqrt{s}} \right)^{A_1^q} \exp(-2A_2^q E_\gamma^*/\sqrt{s})$$

In the CM system the prompt photon distribution will thus appear as if it has an effective temperature:

$$T = \frac{\sqrt{s}}{2A_2^q}$$

for $\sqrt{s} = 200$ GeV, $T = 25$ GeV.

Photon jet fragmentation or Bremsstrahlung

The quark jets, produced by the parton hard scattering, are an additional source of photons, the so-called bremsstrahlung photons. Bremsstrahlung photons result from the fragmentation of quark jets into a collinear photon and a quark. This contribution is important at small p_T and below 4 GeV

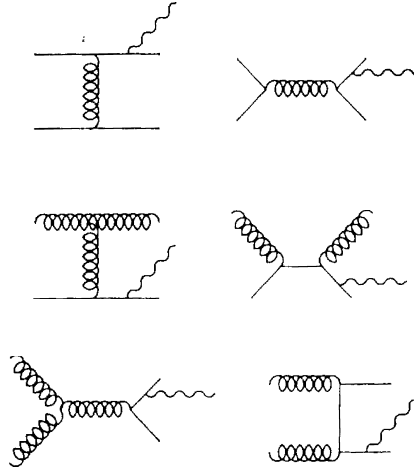


Figure 5.2: *Feynman diagrams leading to a photon (bremsstrahlung) fragmented off a final state quark.*

is comparable to the Compton process at RHIC energies (Figure 5.3) and provides the largest QCD contribution at LHC energies (Figure 5.4).

This production may be modified when jets traverse dense partonic matter. Indeed quark jets suffer a substantial energy loss while propagating through the hot and dense central region. This energy loss is caused by induced gluon radiation. Consequently the fragmentation of the jets into photons with high transverse momenta will be inhibited. This effect is illustrated in Figures 5.5 and 5.6.

These calculations [16] give upper limits for the photon production as very short thermalization time ($\tau_0 = 0.124$ fm/c) and high initial temperatures ($T_0 = 530$ MeV for RHIC and $T_0 = 880$ MeV for LHC) have been considered. They indicate the following:

1. At RHIC prompt photons are the dominant contribution for $k_T \geq 2.5$ GeV and that thermal photons provide the main contribution below $k_T \leq 3$ GeV only when the jets are fully quenched.

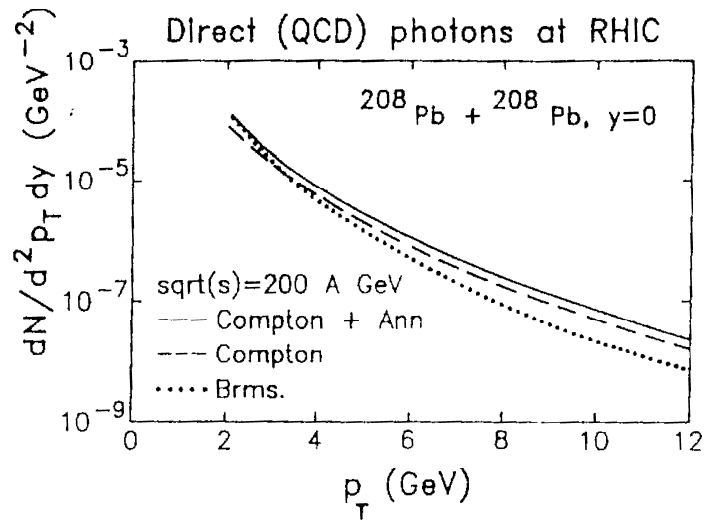


Figure 5.3: The Compton, Compton+annihilation and jet fragmentation contributions to direct photons at RHIC energies at central rapidity for Pb+Pb collisions. From reference [2].

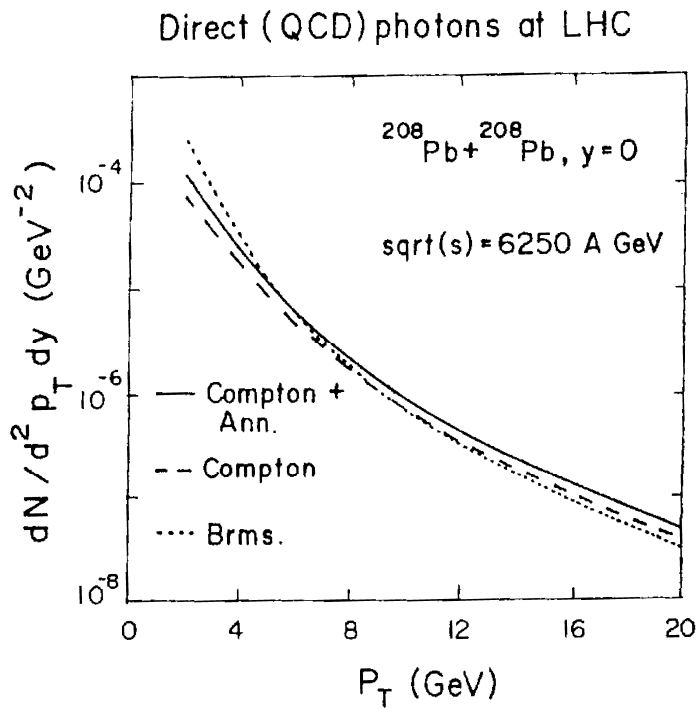


Figure 5.4: The Compton, Compton+annihilation and jet fragmentation contributions to direct photons at LHC energies at central rapidity for Pb+Pb collisions. From reference [2].

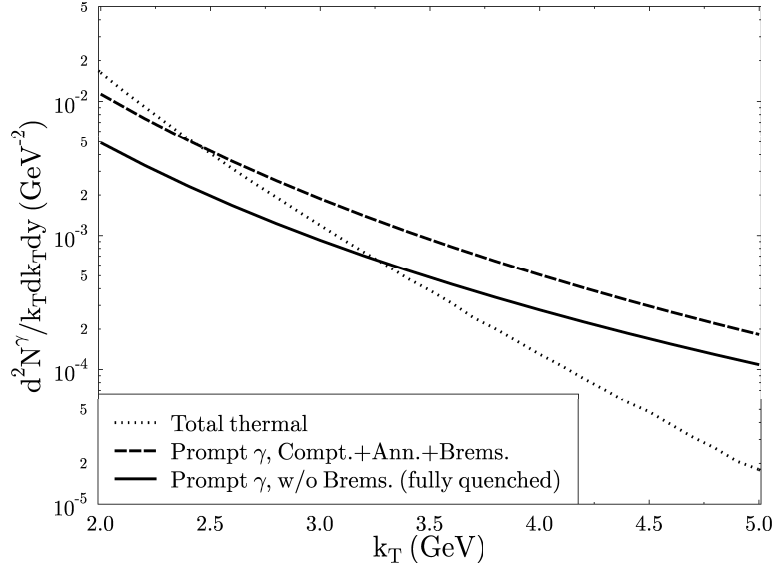


Figure 5.5: Transverse momentum distribution of prompt QCD-photons and thermal photons at mid-rapidity for central Au+Au collisions at RHIC energies. From reference [16].

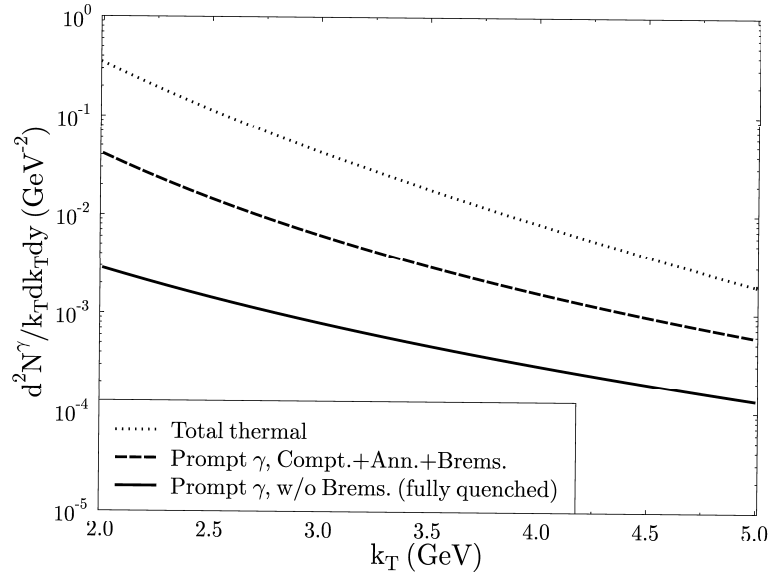


Figure 5.6: Transverse momentum distribution of prompt QCD-photons and thermal photons at mid-rapidity for central Au+Au LHC energies. From reference [16].

2. At LHC, because of the shadowing of the nuclear structure function, the prompt photons might be below the thermal radiation over the whole k_T range.

Anyhow thermal and prompt photon spectra can be distinguished by their different slopes.

5.2.2 Photon production in the quark gluon plasma: thermal photons

Because of the parton energy losses, most of the mini-jets (by definition: a few GeV partons between 1 and 5 GeV) are trapped in the fireball, created in central collisions, and therefore contribute to the equilibration of the quark-gluon plasma. The basic processes are the same as those described previously but now they are governed by the thermal quark and gluon distribution.

- Partons phase-space density:

The time τ_0 when quarks and gluons are first put on mass shell by collisions between the incoming nuclei is called the formation or materialization time; it is of the order of a typical strong interaction time, i.e., 1 fm/c. Gluons may equilibrate much faster because the gluon-gluon cross section is larger than the gluon-quark and quark-quark ones, leading to a chemical relaxation time for gluons smaller than that for quarks. This scenario is called the *hot glue* scenario. The chemical equilibrium for gluons could then be reached at $\tau_0 = 0.3$ fm/c and with temperatures 2 to 3 times larger than the QGP initial temperature. However albeit a thermalization is obtained that early in the reaction, the plasma is not yet in chemical equilibrium. The chemical equilibrium is likely to proceed through gluon multiplication ($gg \leftrightarrow qqg$) and quark production.

At time τ_0 the phase-space density of quarks and gluons has a locally exponential distribution characterized by the temperature T :

$$f_q(E) = \frac{1}{e^{E/T} + 1} \text{ Fermi Dirac distribution for quarks} \quad (5.3)$$

$$f_g(E) = \frac{1}{e^{E/T} - 1} \text{ Bose Einstein distribution for gluons} \quad (5.4)$$

At RHIC $T=500$ MeV photons with $E_T \geq 8$ GeV, and at LHC $T=900$ MeV $E_T \geq 14$ GeV stem from the early phase when the energy density is greatest before the initial phase-space distribution of partons has changed through the expansion of the system.

- Cross section: The basic processes are the same as those of hard scattering and the cross sections are given by Equations 5.1 and 5.2 with the quark distributions now replaced by the thermal distributions of Equations 5.3 and 5.4.

The rate for the production of hard photons evaluated to one loop order using the effective theory based on resummation of hard thermal loops is given by[?] [11]:

$$\frac{E_\gamma dN_\gamma}{d^3p_\gamma d^4x} = \frac{\alpha_e \alpha_s}{2\pi^2} \sum_f (e_f^2) T^2 \exp\left(-\frac{E_\gamma}{T}\right) \ln\left(\frac{cE_\gamma}{\alpha_s T}\right) \quad (5.5)$$

where the constant $c \approx 0.23$ and f denotes the quark flavor and e_f its electric charge.

By extending the evaluation of the photon production in a QGP up to two loops [12] it is found that the bremsstrahlung process gives a contribution which is similar in magnitude to the Compton and annihilation contributions evaluated up to the one loop (Equation. 5.5). The rate due to bremsstrahlung processes is given by:

$$\frac{E_\gamma dN_\gamma}{d^3p_\gamma d^4x} = \frac{8\alpha_e\alpha_s}{\pi^5} \sum_f (e_f^2) T^2 \exp\left(-\frac{E_\gamma}{T}\right) (J_T - J_L) \ln(2) \quad (5.6)$$

where $J_T \approx 4.45$ and $J_L \approx -4.26$ for 2 flavors and 3 color of quarks. For 3 flavor of quarks, $J_T \approx 4.80$ and $J_L \approx -4.52$.

The same authors introduces a new photon production mechanism, the $q\bar{q} \rightarrow \gamma$ annihilation with the scattering. It corresponds to the annihilation of an off-mass shell quark and an anti-quark, where the off-mass shell quark is a product of scattering with another quark or gluon. This process cannot exist in the medium because of momentum conservation which is taken care off by the medium. The contribution of this mechanism is given by:

$$\frac{E_\gamma dN_\gamma}{d^3p_\gamma d^4x} = \frac{8\alpha_e\alpha_s}{3\pi^5} \sum_f (e_f^2) E_\gamma T^2 \exp\left(-\frac{E_\gamma}{T}\right) (J_T - J_L) \quad (5.7)$$

This mechanism completely dominates the emission of hard photons.

A calculation [13] assuming photon emission from a QGP at T=250 MeV is compared to the usual one loop calculation (Figure 5.7). The photon rate is predicted to be at least a factor five more intense when the calculation is performed up to the order of two loop and the dominant mechanism is clearly annihilation with scattering.

5.2.3 Photons emission and collision dynamics

Standard case

At RHIC energies (Figure 5.8) the QGP photons spectrum has the following properties:

- The transverse expansion of the plasma leaves the thermal photon production at RHIC essentially unchanged for $p_t > 1$ GeV.
- Prompt photons will dominate the yield beyond $p_t \geq 4$ GeV.

At LHC energies (Figure 5.9) the QGP photons spectrum has the following properties:

- The production of thermal photons with large p_t remains unchanged as they have origin in the early hot stages, when the flow effects are still small.
- The production of low p_t photons decreases considerably due to reduction in the space-time volume occupied by colder matter in the presence of transverse expansion.
- While the prompt photon production may remain lower than the thermal photon yield up to $p_t = 5$ GeV, the background contribution of photons fragmented off high- p_t quark jets is large.

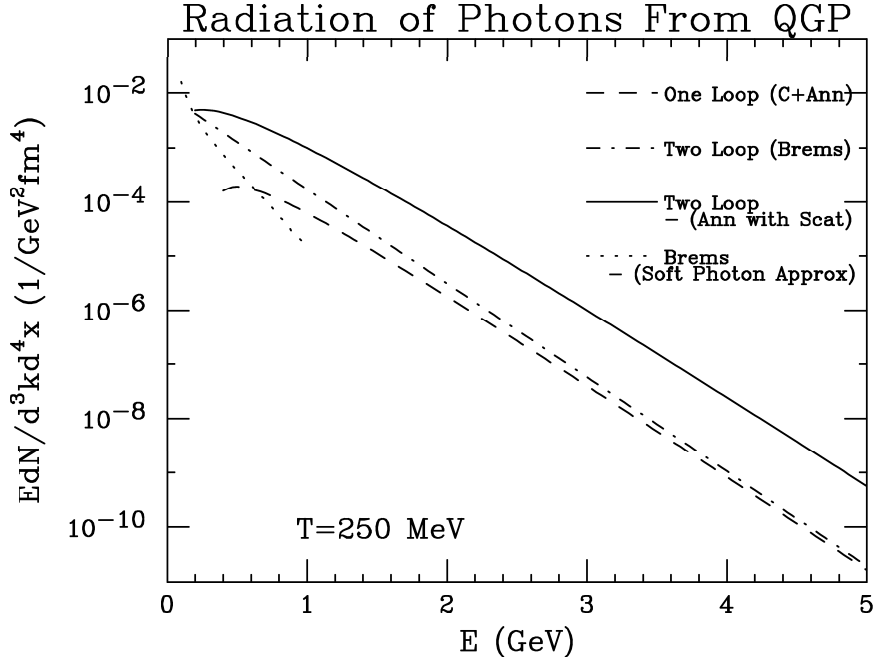


Figure 5.7: Photon production rate calculated for the emission from a QGP at $T=250$ MeV. The rate associated with the processes calculated at the order of one loop are derived from Equation 5.5, the two loop calculation for bremsstrahlung is derived from Equation 5.6 and for annihilation with scattering from Equation 5.7. From reference [13].

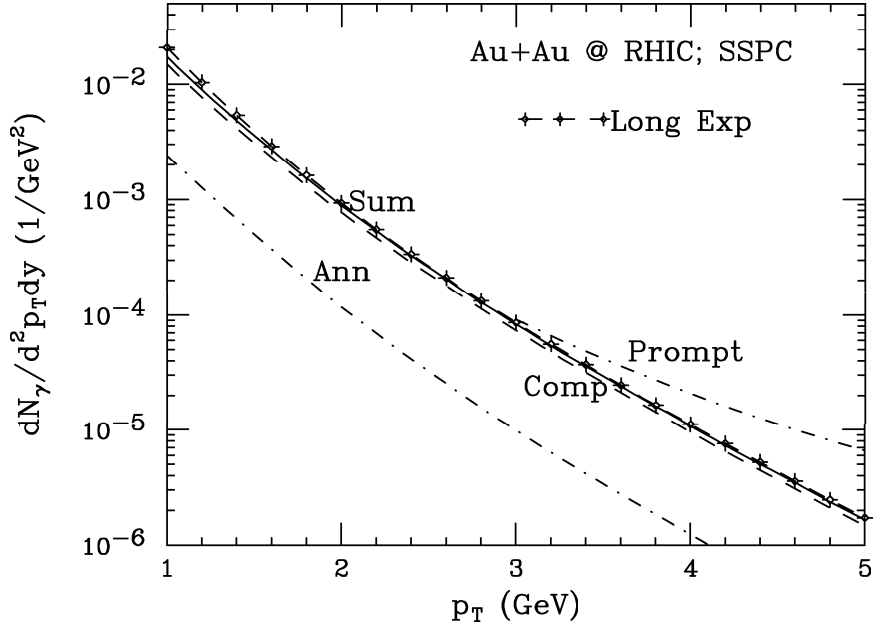


Figure 5.8: Distribution of thermal photons from the QGP phase at RHIC. The Compton and annihilation yields and their sum are shown for the case with transverse expansion. Results are also given for a purely longitudinal flow. Prompt photons, whose production is governed by structure functions, are seen to dominate the yield for momenta larger than 3-4 GeV. From reference [5].

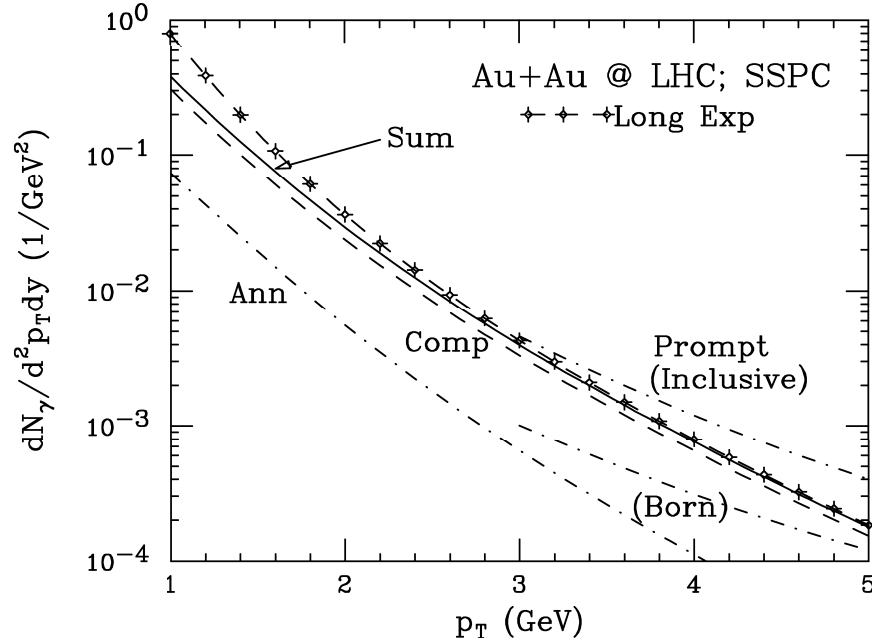


Figure 5.9: Same as previous figure at LHC. The prompt photons from fragmentation of quark jets are also shown. From reference [5].

Hot -glue scenario

Within the hot-gluon scenario [15] the amount of thermal photons in the transverse momentum range between 3-5 GeV is considerably enhanced (Figure 5.10), due to the much higher initial temperature. This provides a window of opportunity to observe the QGP signal.

- In the figure the photon spectra have been calculated assuming an hydro-dynamical expanding plasma (f_q evolves according the relativistic Boltzmann equation plus a collision term; photons are produced perturbatively), and assuming a free-streaming plasma (the collision term is omitted). The two distributions are equal at the highest transverse momentum a consequence of the fact that f_q has not yet evolved from the initial distribution when these energetic photons are produced.

5.2.4 High mass di-photons

As large mass di-leptons, large mass di-photons have their origin in the hot and dense stage of QGP and their detection would provide information about the state of matter [17]. Comparison with di-lepton data would confirm the result. Di-photons are produced through quark-antiquark annihilation during the initial stage as well the thermalizing stage of the heavy-ion collision. Like for di-leptons, the measurement of di-photons has the advantage that the mass spectrum is only influenced by the temperature during the collision history and is not affected by collective flow.

For di-photon masses, M , much larger than the mass of the quarks:

$$\sigma_{qq}^{\gamma\gamma}(M) = 2\pi\alpha^2 N_c (2S + 1)^2 \sum_q \frac{e_q^2}{M^2} \ln\left(\frac{M^2}{2.718m_q^2}\right)$$

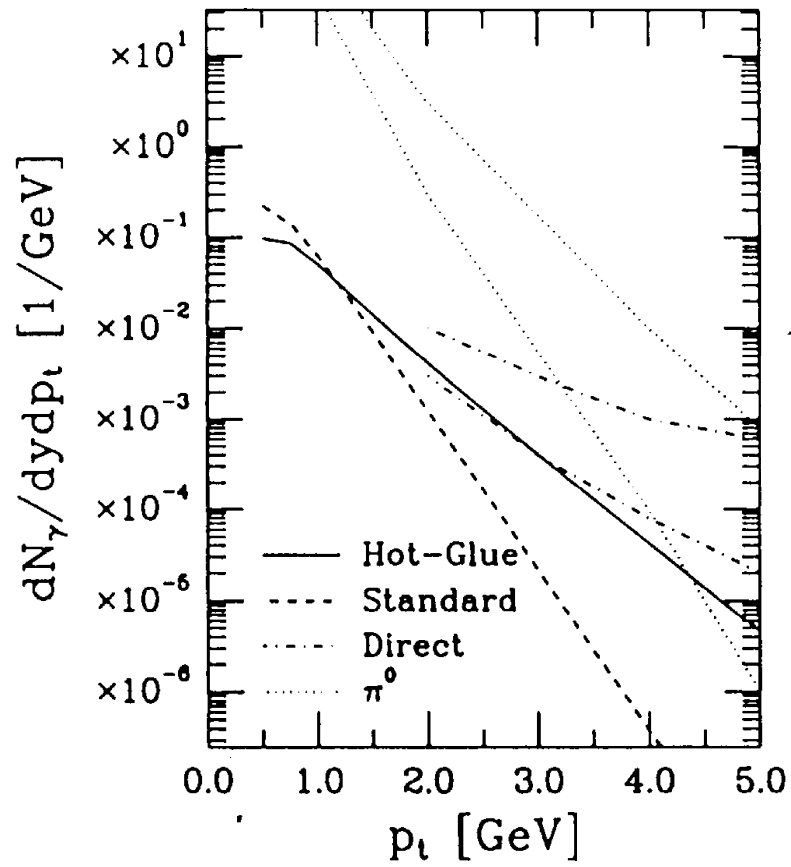


Figure 5.10: The transverse momentum distribution of photons, produced from quark-gluon plasma. Hot glue implies $\tau_0 = 0.3 \text{ fm}$, $T_0 = 460 \text{ MeV}$; Standard $\tau_0 = 1 \text{ fm}$, $T_0 = 240 \text{ MeV}$; Direct represents the contribution from all sources and π^0 denotes the range of decay photons. The system is Au+Au at 200 GeV. From reference [15]

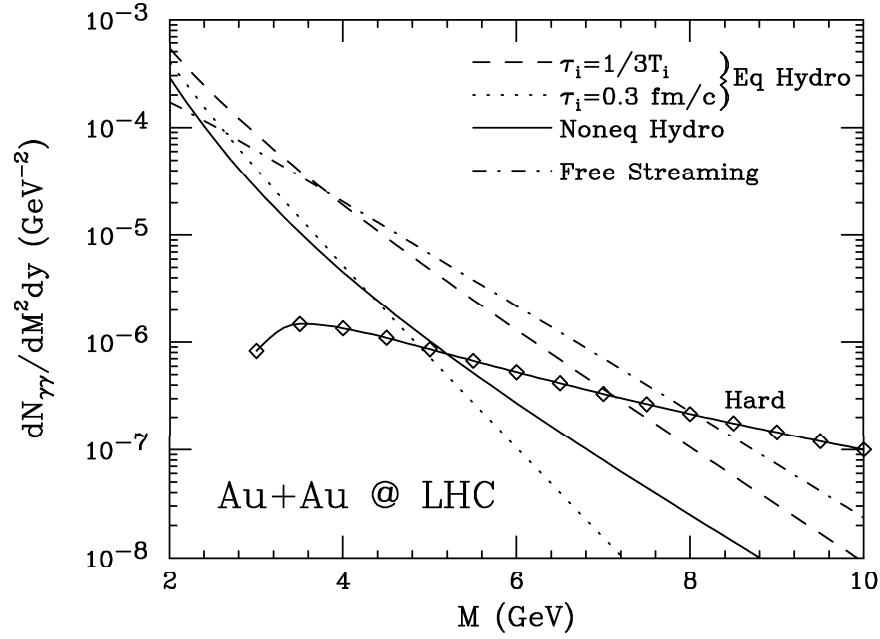


Figure 5.11: Invariant mass distribution of photon pairs from quark-antiquark annihilation for the Au+Au system at LHC energies in a fully equilibrated QGP (Eq. Hydro), a free-streaming gas of quarks and gluons, and a chemically equilibrated (Noneq. Hydro) quark gluon system. Invariant mass distribution of hard photon pairs (Hard) from initial quark-antiquark annihilation for momentum transfer greater than 2 GeV is also shown. From reference[17]

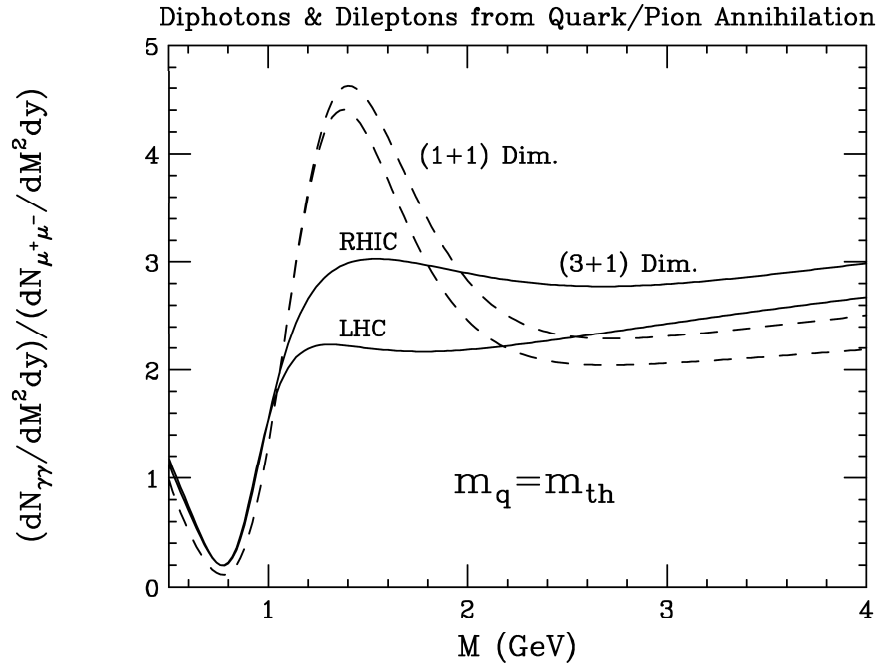


Figure 5.12: Ratio of di-photon and di-lepton invariant mass distribution for a hadronizing QGP at RHIC and LHC energies. From reference [17].

with $N_c = 3$, $S = 1/2$ and e_q the charge of the quark. The quarks in a heat bath acquire a thermal mass:

$$m_{th} = \sqrt{2\pi\alpha_s}/3T$$

and $m_q = m_{th}$ is assumed.

Calculations have been performed within different assumptions:

- equilibrated hydrodynamic evolution starting at $\tau_0 = 1/3T_0$ and $T_0 = 860$ MeV for LHC energies;
- free-streaming evolution starting with the same values as above;
- non-equilibrium hydrodynamic evolution starting at $\tau_0 = 0.3$ fm/c;
- hard QCD annihilation with a cut-off on the momentum transfer at 2 GeV.

It is found that thermal di-photons dominate the spectrum up to 6 GeV at LHC. The limit is found to be 4 GeV at RHIC.

To compare the di-photon spectrum with the di-lepton spectrum all mechanisms for the production of direct photons have been taken into account plus, in addition, the annihilation of pions in hadronic matter into a di-photon or a di-lepton. The ratio of di-photons to di-leptons is plotted in Figure 5.12 as a function of the invariant mass. The structure around 800 MeV comes from the ρ -meson peak in the pion form factor. The maximum around 1.4 GeV corresponds to the region where the structureless quark annihilation process starts dominating. Since it was assumed that the thermal mass of quarks depends on the temperature and enters the cross section through the factor $\ln(M^2/2.7m_q^2)$, the ratio at large mass might reveal information of dynamics and confirm the temperature dependence of the thermal mass of quarks.

Comparing the single photon production with the di-photon production could be an approach to establish the existence of the hot glue scenario (see 5.2.3). Single photons as we know are produced through quark annihilation and gluon Compton scattering whereas di-photon are produced through quark annihilation only. Thus to the leading order the di-photon production rate is determined by the quark distribution whereas the single photon production is sensitive to both quark and gluon distribution. The relative production rates of photons and di-photons has been calculated within the hydrodynamical model including a phase transition (Figure 5.13). One observes that at masses larger than about 3 GeV, i.e., for photons from the pre-equilibrium phase, the Compton cross section decreases (lower curve decreases) and that the annihilation has become the dominant contribution (upper curve increases). If in experiments the saturation of the photon to di-photon ration is indeed observed at high masses, it would indicate that the gluon component continues to be important and we can obtain information about the glue distribution from simultaneous measurement of photons and di-photons.

5.2.5 Photon production in the hadronic gas

Hot and dense matter expands and cools: photons are produced in the warm, transversally expanding hadronic matter. The photon spectrum follows the hadron distribution with a slope given by the hadron-gas temperature. The spectrum can be modified by a possible rapid expansion of the gas. The main processes are:

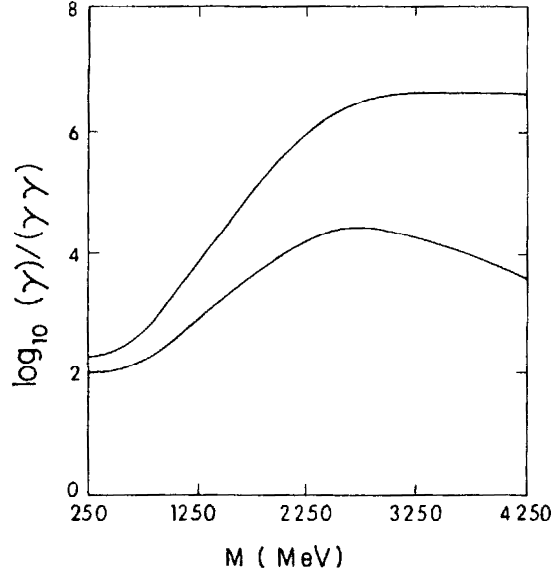
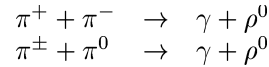


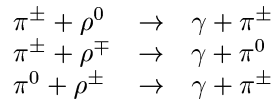
Figure 5.13: Ratio of photon to di-photon count rates as a function of $M \sim p_T$. The upper curve is for both Compton and annihilation channels for single photon while the lower curve is for Compton alone. The time at which gluon thermalize is much earlier than the overall equilibration time $\tau_g = \tau_0/20$, the QGP temperature is taken as $T=200$ MeV. From reference [2].

Elementary processes

1. Annihilation:



Compton scattering:



This former process is the dominant one. Its cross section in the case where photon energies are much large than the hadron masses is:

$$\begin{aligned} E_\gamma \frac{dN_{(\pi\pi \rightarrow \gamma\rho)}}{d\vec{p}_\gamma^3 d^4x} &= \frac{1}{(2\pi)^5} f_\pi(\vec{p}_\gamma) \int ds \frac{dE_\pi}{4dE_\gamma} f_\pi(E_\pi) [1 + f_\rho(E_\pi)] \\ &\quad \times \sqrt{s(s - 4m^2)} \sigma_{\pi\pi \rightarrow \gamma\rho}(s) \end{aligned}$$

The hadron phase-space density $f_\pi(p_\pi)$ for high photon energies is described by an exponential form: e^{-E/T_π} . $T_\pi = 260$ MeV at RHIC, and 330 MeV at LHC.

It has been shown [19] that the $\pi\rho$ channels proceeds mainly through the A_1 resonance. The rate of photon production can be parametrized by the following analytical function::

$$E_\gamma \frac{dN_{(\pi\rho \rightarrow A_1 \rightarrow \pi\gamma)}}{d\vec{p}_\gamma^3} = 2.4T^{2.15} \exp \left[-1/(1.35TE_\gamma)^{0.77} - E_\gamma/T \right]$$

Results

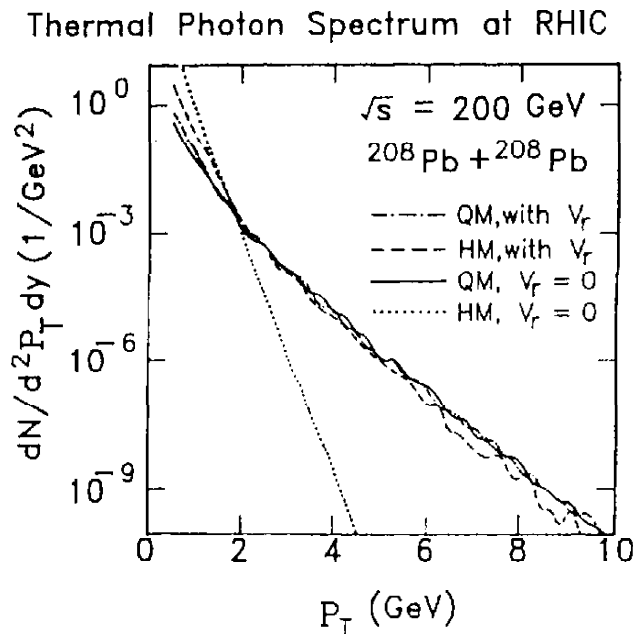


Figure 5.14: Spectrum of thermal photons emitted from an expanding QGP up to the time of freeze-out at RHIC energies with and without transverse flow: $T_i = 532$ MeV, $\tau_i = 0.124$ fm/c, $dN/dy_\pi = 1735$, $T_c = 160$ MeV and $T_F = 100$ MeV. The hadronic matter is composed of π , ρ , ω , and η mesons. The quark matter is composed of u and d quarks and gluons. From reference [2].

The cross section for photons stemming from the plasma is larger than the cross section for photons from the hadron gas at transverse energies larger than 2 GeV at RHIC as well as at LHC, because high energy photons come predominantly from the matter with the highest temperature. HOWEVER if there is transverse flow in the hydro-dynamical expansion, photons from the cooler hadronic phase are Lorentz boosted to higher momentum so that the distribution of photons from the plasma and the hadron gas are the same even at high photon energies (see Figures 5.14 and 5.15)! Note that di-leptons or di-photons do not have this problem (their mass is Lorentz invariant).

5.2.6 Decay photons

A major contribution to the photon spectrum originates from the two photon decay of neutral pion and η meson decay which occurs about 10^7 fm/c after the beginning of the collision. This contribution represents the major problem in a photon experiment and must be subtracted to give access to the direct photon spectrum of interest. therefore the neutral meson momentum distribution must be known accurately. This represents an experimental challenge. It is considered that a direct to photon ratio of or larger than 10% is required to extract safely the direct photon spectrum (see Figure 5.16).

To illustrate on a more global basis the decay-photons contribution to

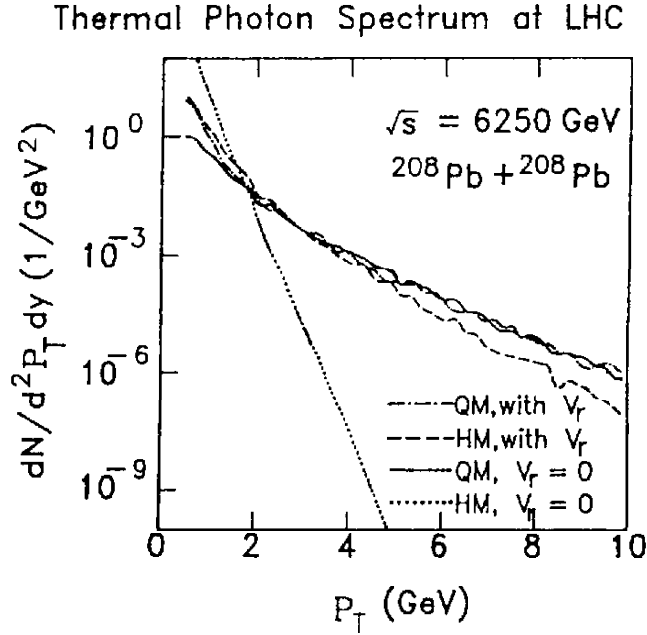


Figure 5.15: Spectrum of thermal photons emitted from an expanding QGP up to the time of freeze-out at RHIC energies with and without transverse flow: $T_i = 958 \text{ MeV}$, $\tau_i = 0.069 \text{ fm}/c$, $dN/dy_\pi = 5624$, $T_c = 160 \text{ MeV}$ and $T_F = 100 \text{ MeV}$. The hadronic matter is composed of π , ρ , ω , and η mesons. The quark matter is composed of u and d quarks and gluons. From reference [2].

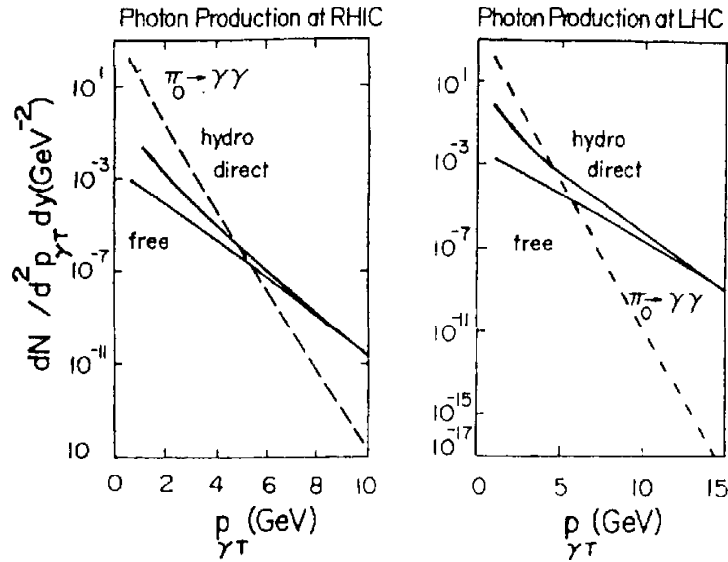


Figure 5.16: Photon spectra from hydro-dynamical expanding and free streaming QGP, for RHIC energies ($dN/dy=1735$, $T_0=500 \text{ MeV}$) and LHC energies ($dN/dy=5624$, $T_0=500 \text{ MeV}$). The π^0 p_T spectrum is assumed to be exponential with inverse slope of 260 MeV at RHIC and 330 MeV at LHC energies. From reference [2].

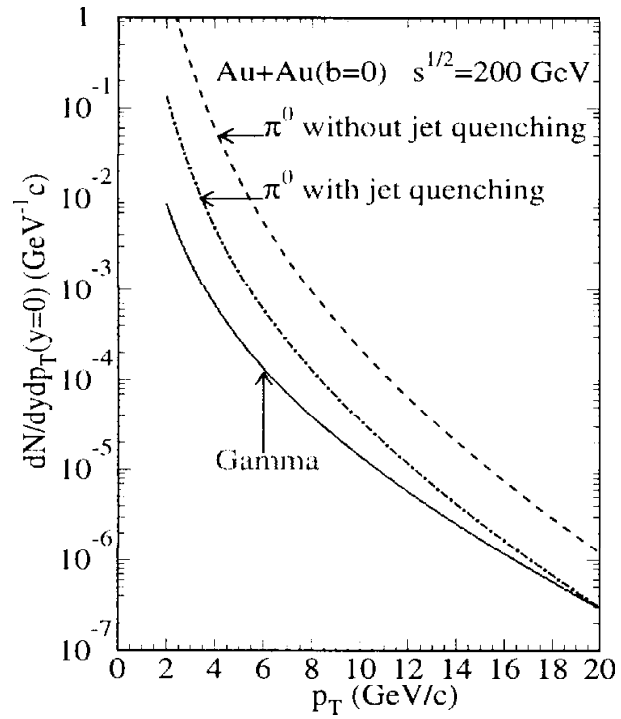


Figure 5.17:

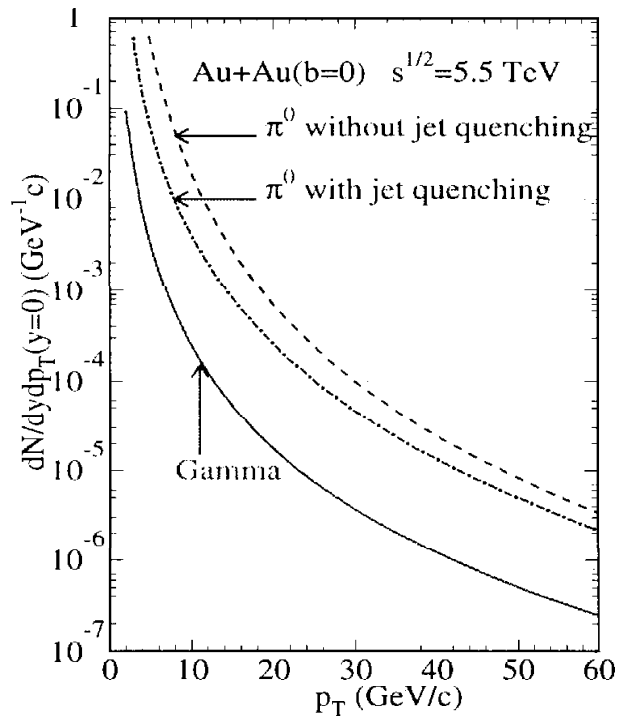


Figure 5.18:

the photon spectrum, the scaling behavior of the number of direct photons with the number of charged particles produced in heavy-ion collisions.

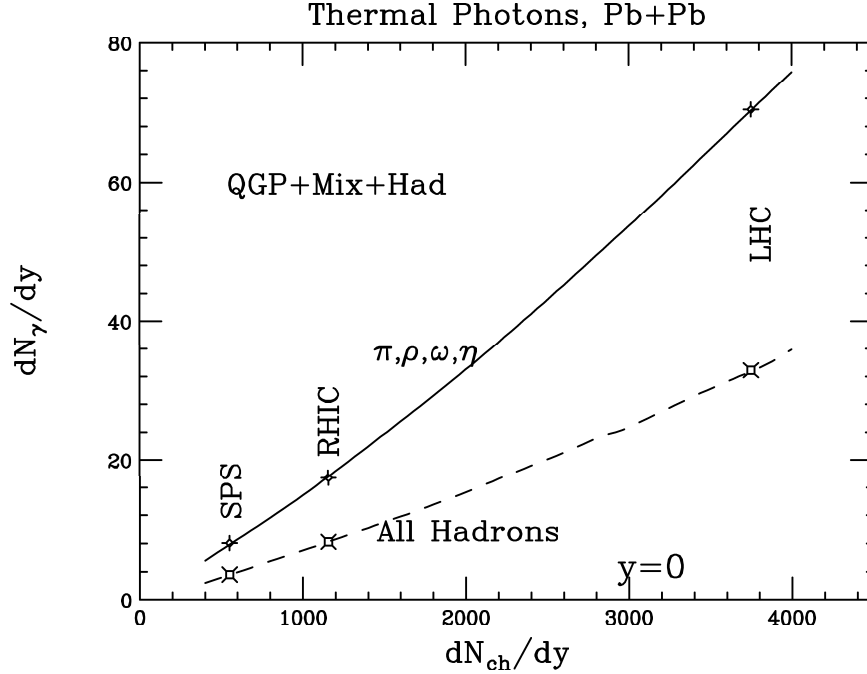


Figure 5.19: Variation of rapidity density of thermal photons with the charged particle rapidity density with two EOS (the number of hadrons changes) involving phase transition.

It is found that the number of photons scales as $N_{ch}^{1,2}$ with a constant of proportionality decided by the EOS.

5.3 Concluding remark on direct photons

Photons coming from direct parton interactions early in the collision may out-shine photons coming from meson decays at the end of the collision for transverse energies larger than 5 GeV and for central collisions at RHIC and LHC. A hadron gas shines as brightly as (or even slightly brighter than) a quark-gluon plasma. The occurrence of a QGP will be accompanied by photons with a greater temperature. A photon distribution exhibiting a much higher temperature may allow one to distinguish the QGP source from the colder hadron source. But transverse expansion of the warm hadronic matter towards the end of the collision can boost locally soft photons to higher transverse momentum. The photon yield from parton collisions will be greater than the photon yield from the QGP at large photon energies. This picture might be dramatically modified if it is confirmed that taking into account two loop processes in the calculation of the elementary photon production rates as discussed in section 5.2.2. Including this new development the spectra shown in Figure 5.20 for RHIC energies and Figure 5.21 for LHC energies were obtained [13]. It is assumed that a chemically and thermally equilibrated quark-gluon

plasma is formed at $\tau_0 = 0.5$ fm/c with a temperature of 310 MeV at RHIC energies and 450 MeV at LHC energies deduced from the Bjorken condition. The phase transition temperature is taken at 160 MeV and the freeze-out temperature at 100 MeV. The history of the evolution of a central lead on lead collision is obtained by solving the hydrodynamic equations including the three phases: QGP, mixed and hadronic. The pre-equilibrium contributions cal-

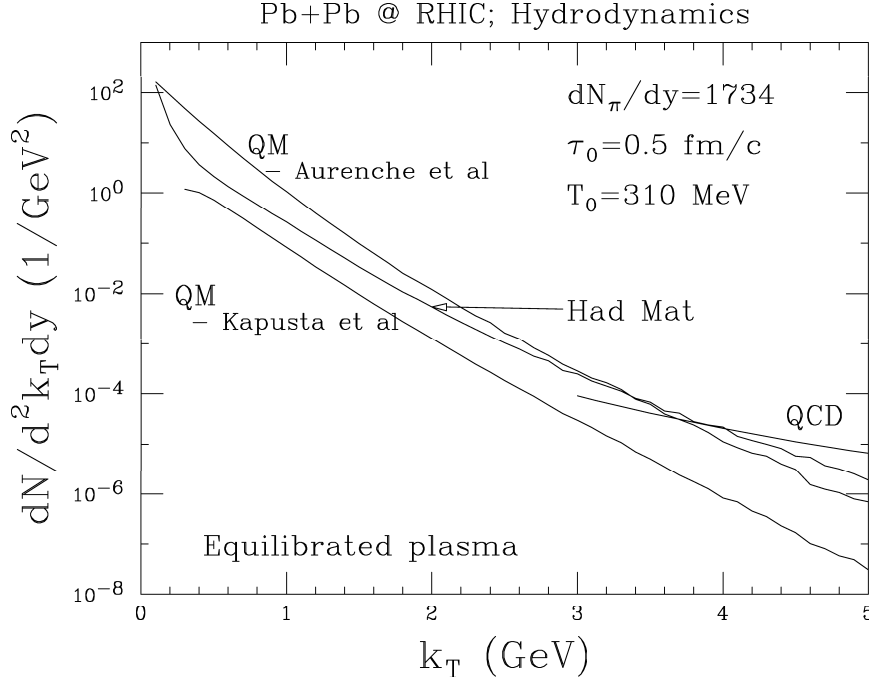


Figure 5.20: Radiation of photons from central collision of lead nuclei at RHIC energies from the hadronic matter (in the mixed phase and the hadronic phase) and the quark matter (in the QGP phase and the mixed phase). The contribution of the quark matter while using the rates obtained by calculation at the order of one loop and two loop and those from hard QCD processes are shown separately. From reference [13]

culated within the parton cascade model [5] but with elementary cross sections evaluated at the order of one one loop only has been added to the figures. The results for RHIC energies indicate that within a window extending up to almost 3 GeV the thermal photons from the QGP out shine the hadronic contribution. At LHC energies this window extends to beyond 4 GeV. Therefore this result provide the exciting possibility that the quark matter may emit photons which have intensities almost an order of magnitude larger than those coming from hadronic matter over a fairly wide window. The pre-equilibrium contribution at larger transverse momentum would even substantially widen this window.

With which energy and when during the collision photon shine and what can be learned from this subtle light is illustrated by the cartoon in Figure 5.22G. David and P. Stankus. Meditate!

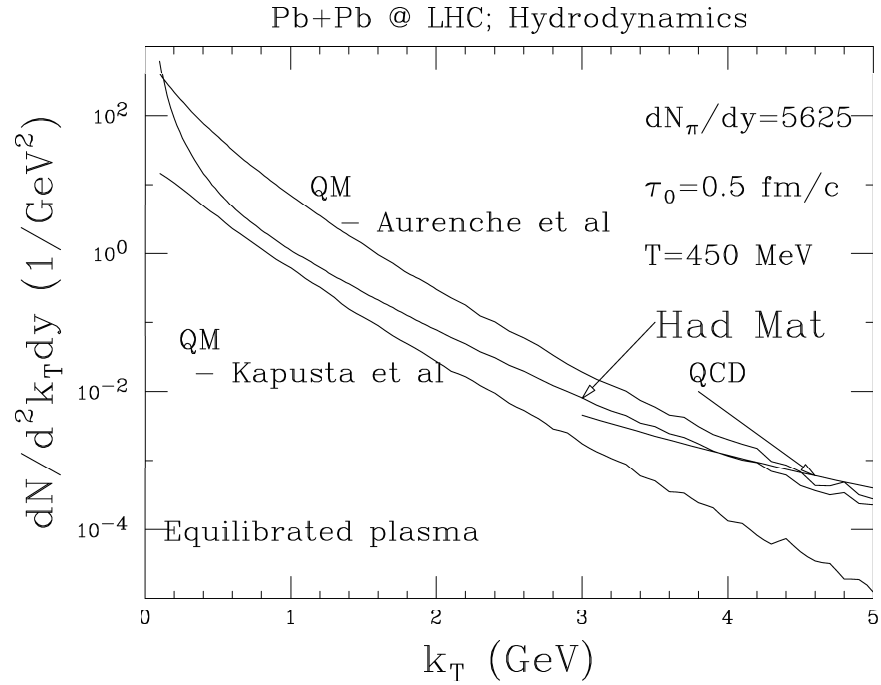


Figure 5.21: Same as Figure 5.20 for LHC energies. From reference [13].

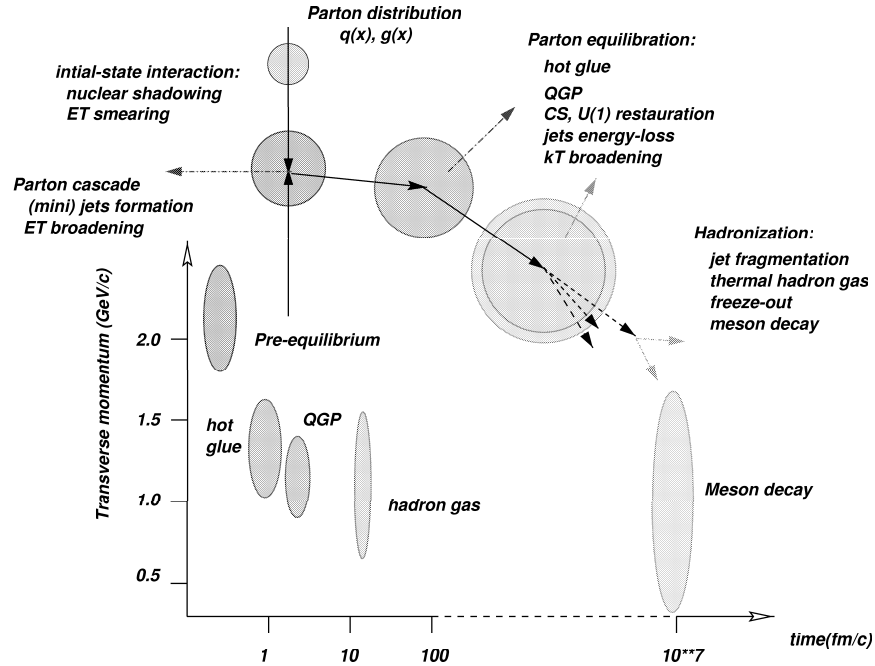


Figure 5.22: Inspired by a cartoons from Gabor David (BNL) and Paul Stankus (ORNL).

5.4 Photon interferometry

We have learned that direct photons are emitted at all stages of the heavy-ion collisions. Measuring the photon spectrum, which represents the time integrated yield of all direct photons, does not permit to distinguish the various contributions. It is however possible to distinguish the early photon component, associated to the rapidly developing parton cascade, from the rest by exploring the emission time information which is imprinted into the two-photon correlation pattern.

5.4.1 Photon statistics in quantum optics

Quantum optics tells us that the statistics of photons behaves differently depending on the nature of the source (Figure 5.23). In case of a coherent source, like a laser, the number of photons measured during a time t are statistically distributed according to the Poisson law:

$$P(n) = \frac{\langle n \rangle^n}{n!} e^{-\langle n \rangle}$$

where $P(n)$ is the probability to measure n photons and $\langle n \rangle$ is the average number of photons measured during time t . In case of a chaotic source, like a light bulb, which emits photons according to a Gaussian distribution and for which the coherence time, τ_c , is larger than the measurement time, the number of detected photons are distributed according to a Bose-Einstein distribution:

$$P(n) = \frac{\langle n \rangle}{(1 + \langle n \rangle)^{n+1}}$$

In a light-source atoms emit wave packet with a random phase-relation, i.e., incoherently. The length of such a wave packet is defined as the coherence length, L_c , and is proportional to the inverse of the spectral width of the emitted light. When the time difference between two wave packets is smaller than the coherence length, $\tau_c = L_c/c$, the packets are coherent, i.e., they have a constant phase relation.

A way to determine if a light source is a laser or a thermal source with a very narrow band width consists in measuring the second order correlation function (see for example reference [21]). The correlation function is obtained from the probabilities that photons arrive in coincidence at two photon detectors as a function of the arrival time difference (Figure 5.24).

For a chaotic source at a coincidence time $\tau = 0$, the number of coincidences is larger than at coincidence times larger than the coherence time. This can be interpreted by the fact that photons emitted by a chaotic source have the tendency to arrive in packets to the detector whereas the photon emission by a laser is regular. It is important to note that the statistics distribution is a property of the source and not of the photons.

5.4.2 Application to particle and nuclear physics

The property of Bose-Einstein statistics of photons can be generalized: statistical fluctuations of a chaotic system consisting of identical non-interacting bosons in the six-dimensional phase-space are not Poissonian but of Bose-Einstein type. To find at which scale the statistical behavior of identical bosons changes from a Poisson distribution to a Bose-Einstein distribution one can, for example, measure the two-particle correlation as

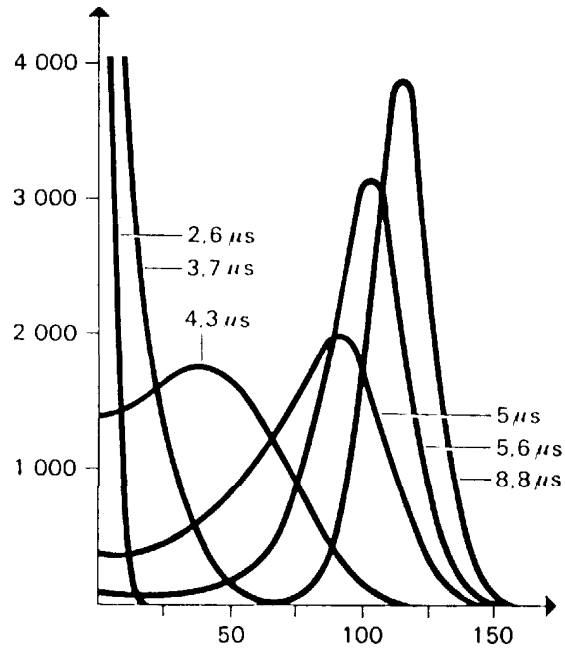


Figure 5.23: *Statistical distributions of photons detected at different times following the startup of the laser oscillation. At short times the source is chaotic and the distribution is of Bose-Einstein type. At longer times the source is a laser and the distribution becomes Poissonian. Form reference [20].*

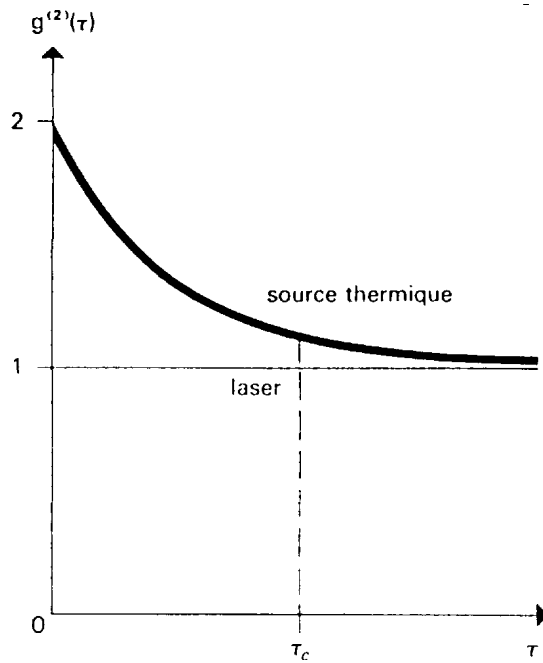


Figure 5.24: *Second order correlation function. For a thermal source there is an augmentation of the coincidence rate when the coincidence time is smaller than the coherence time. From reference [20].*

a function of the considered phase-space volume. This technique was first developed by Hanbury-Brown and Twiss and applied to the measurement of the apparent size of stars, hence the name of HBT correlations, also known as Bose-Einstein correlations (BEC). Another method consists in studying directly the count probability statistics as a function of the momentum or to study moments like factorial moments. This is the only method applicable to multi-particle correlations.

In particle physics the same technique was first applied by Goldhaber, Goldhaber, Lee and Pais (the GGLP effect) to study the correlation between charged pions emitted in $p\bar{p}$ collisions. It has now become a common technique in particle and nuclear physics. There the space-time configuration is unknown, whereas the momentum space is accessible to measurement. The goal of a correlation measurement is to find the scale in the accessible coordinate of the phase-space for which the fluctuations become of Bose-Einstein type. The scale of the system along the unaccessible coordinates is then deduced from the phase-space volume corresponding to a single phase-space cell:

$$\Delta x \Delta p \sim \hbar^3$$

The correlation function

The correlation function is defined as the ratio of the probability for the coincidence of two particles with four-momentum k_i relative to the probability of observing the particles individually:

$$C_2(k_1, k_2) = \frac{P(k_1, k_2)}{P(k_1)P(k_2)}$$

One can show that for an extended chaotic source the correlation function for identical non-interacting bosons is directly related to the Fourier transform of the density distribution of the particles emitting source:

$$C_2(k_1, k_2) = 1 + |\tilde{\rho}(q; k_1 k_2)|^2$$

The source density is usually parametrized in the form of a Gaussian distribution:

$$\rho(x; k_1 k_2) = \frac{\mathcal{N}}{4\pi^2 R_x R_y R_z \sigma_t} \exp \left\{ -\frac{x^2}{2R_x^2} - \frac{y^2}{2R_y^2} - \frac{z^2}{2R_z^2} - \frac{t^2}{2\sigma_t^2} \right\}$$

and the Fourier transform is:

$$\rho(q; k_1 k_2) = \mathcal{N} \exp \left\{ -\frac{R_x^2 q_x^2}{2} - \frac{R_y^2 q_y^2}{2} - \frac{R_z^2 q_z^2}{2} - \frac{\sigma_t^2 t^2}{2} \right\}$$

and the correlation function writes:

$$C_2(k_1, k_2) = C_2(q; k_1, k_2) = 1 + \mathcal{N} e \left(-R_x^2 q_x^2 - R_y^2 q_y^2 - R_z^2 q_z^2 - \sigma_t^2 t^2 \right)$$

In general \mathcal{N}, R_i and σ_t are parameters function of k_i . However in the particular case where the source is uniform, i.e., the production amplitude at various source points is independent of the source point coordinate then:

$$\rho(x; k_1 k_2) \equiv \rho(x)$$

and

$$C_2(q; k_1, k_2) \equiv C_2(q) = 1 + |\tilde{\rho}(q)|^2$$

In this case the momentum correlation function is related to the Fourier transform of the space-time distribution of the source.

In a heavy ion collisions the particle source expands. The Bose-Einstein correlation is only frozen in at the decoupling time (freeze out time) when the dimensions of the system exceed the pion mean free path. If particles are created at a formation time t_0 , at t_f the particles with a given relative momentum Δp and originally separated spatially by $\Delta x \sim \hbar^3/\Delta p$ are separated by a distance $\Delta x \gg \hbar^3/\Delta p$ and are therefore not correlated. Therefore only particles emitted with a given Δp from a smaller relative distance demonstrate correlation.

Momentum coordinates

To analyze the experimental correlation function one usually decomposes the relative 3-momentum $Q = k_1 - k_2$, into longitudinal (along the beam direction), transverse side ward and transverse outward components:

$$Q_L = (k_1 - k_1)$$

$$Q_S = \frac{Q_T \wedge k_T}{|k_T|}$$

$$Q_O = \frac{Q_T \cdot k_T}{|k_T|}$$

where $k_T = (k_{1T} + k_{2T})/2$ and $Q_T = k_{1T} - k_{2T}$. Assuming the source distribution in Gaussian in the 3 directions, the correlation function writes within this parametrization:

$$C_2(Q_S, Q_O, Q_L) = 1 + \lambda e^{(-Q_S^2 R_S^2 - Q_O^2 R_O^2 - Q_L^2 R_L^2)}$$

Notice here that the time dependence has disappeared!

An other parametrization often used because more convenient and less degree of freedom. The information is also limited. One uses the invariant mass as momentum coordinate:

$$Q_{inv}^2 = (k_1 - k_2)^2 = (k_1^0 - k_2^0)^2 - (\vec{k}_1 - \vec{k}_2)^2$$

with the correlation function:

$$C_2(Q_{inv}) = 1 + \lambda e^{-R_{inv}^2 Q_{inv}^2}$$

The quantity R_{inv} is not a direct measure of the size of the density as it contains also the time component. It is useful in photon-photon correlation measurements because it enables to localize clearly the resonances like neutral pions.

Note that in the two previous expression of the correlation function the parameter λ was introduced. For a fully incoherent source $\lambda = 1$ for hadrons and $\lambda = 0.5$ for photons. These values drop when the source is partially incoherent hence the denomination coherence factor. Experimentally this parameter contains also all the effects which tend to decrease the correlation like random coincidences, etc...

5.4.3 Photon-photon correlation

The two photon correlation function is certainly the most easy to understand since photons are not subject to final state interaction. However it is also at the same time the most difficult to measure for many reasons: photons are rarely produced, the overwhelming background of decay photons makes the correlation signal extremely weak, the conversion of photons into two electrons will populate the correlation function at small relative momenta, photons are emitted during all stages of the collision which introduces complexity in the interpretation of the correlation function. However the last remark can be taken positively. Indeed at variance of the hadrons which probe on the system at freeze out, photons carry information on the pre-equilibrium quark-gluon plasma, the fully equilibrated plasma, the phase transition or mixed phase and the hadronic matter.

An ideal two-photon correlation would look like the one sketched in Figure 5.25.

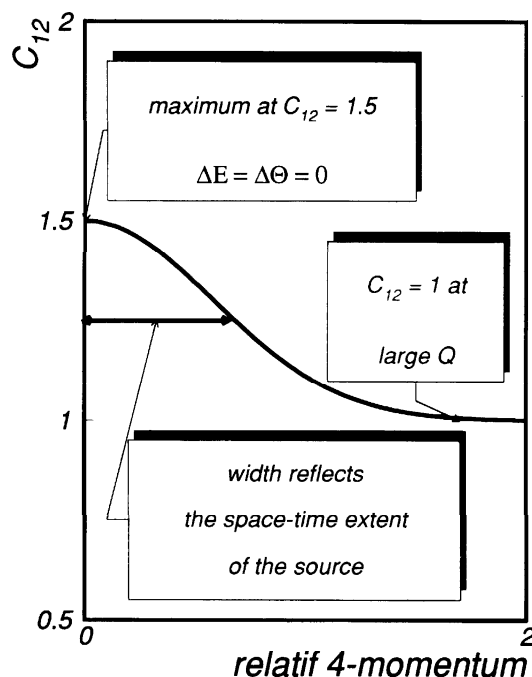


Figure 5.25: *Idealized two-photon correlation function. The magnitude of the correlation is limited to $\lambda = 0.5$ to take into account the polarization of photons.*

For photons produced during an ultrarelativistic collision, including the time dependant photon sources (pre-equilibrium, QGP, mixed and hadronic phases) a covariant form of the correlation function has been derived[24] as:

$$C_2(k_1, k_2) = \int d^4x_1 d^4x_2 w\left(x_1, \frac{k_1 + k_2}{2}\right) w\left(x_2, \frac{k_1 + k_2}{2}\right) \cos(\Delta x^\mu \Delta k_\mu) \quad (5.8)$$

where $w(x, p)$ describe the photon production rates.

We shall now examine the various contributions which will modify the ideal situation:

Resonance decay

For π^0 and η meson the two-photon decay contribution to the correlation function can well be identified as it easily localized in the relative-momentum space (Figure 5.26). The decay of the neutral K meson, $K_s^0 \rightarrow$

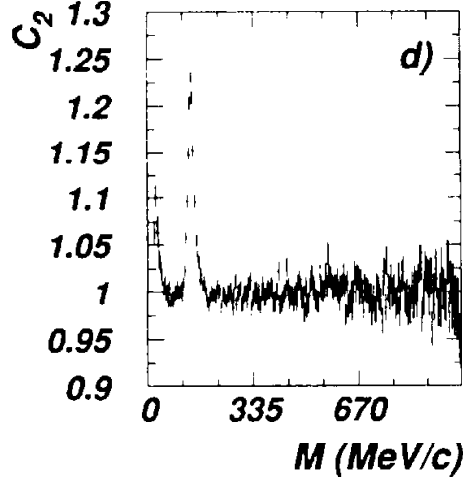


Figure 5.26: Two-photon correlation function measured in the reaction S+Au at 200A GeV by the WA80 collaboration. From reference [22]

$\pi^0\pi^0 \rightarrow \gamma\gamma\gamma\gamma$, can be localized and carry a correlation which however only slightly modifies the two-photon correlation function for radii of the order of 1fm.

Residual $\pi^0 - \pi^0$ correlations

Since most of the photons originate from π^0 decay, the two-photon correlation may carry a residual correlation since pions will them self be correlated. This can be turned to our advantage. It is within the present identification techniques impossible to identify neutral pions on an event by event basis and consequently impossible to construct the correlation function. It was discussed if the pion correlation could indeed be extracted from the measured photon correlation which writes:

$$C_{\gamma\gamma}(\Delta) = \frac{\int F_{\pi}(k_1) F_{\pi}(k_2) C_{\pi\pi}(0.5|k_1 - k_2|) d\rho}{\int F_{\pi}(k_1) F_{\pi}(k_2) d\rho} \quad (5.9)$$

with the following definitions: k_i is the pion 4-momentum which decays into two photons of momentum k_{i1} and k_{i2} , $\Delta = 0.5(k_{i1} - k_{i2})$ is parallel to z and $s = k_{i1} + k_{i2}$, $C_{\pi\pi}$ is the two-pion correlation function and the volume cell is:

$$d\rho = d^3k_1 d^3k_2 d^3s \times \delta\left(\sqrt{m^2 + k_1^2} - \left|\frac{1}{2}s - \Delta\right| - \left|k_1 + \Delta - \frac{1}{2}s\right|\right) \\ \times \delta\left(\sqrt{m^2 + k_2^2} - \left|\frac{1}{2}s - \Delta\right| - \left|k_2 - \Delta - \frac{1}{2}s\right|\right)$$

where the δ functions ensure energy conservation at the decay vertex. Having the measured two-photon correlation it is sufficient(!) to inverse the integral in Equation 5.9 to obtain the two-pion correlation function.

This can only be done numerically [23]. Why should one go through that much of pain? Because π^0 are a much better probe as the commonly used charge pions as they are not affected by the time-dependent Coulomb field in the expanding system which modifies in a rather uncontrolled way the charged pion correlation function. Results from simulations (Figure 5.27) one can conclude:

Fig. 1

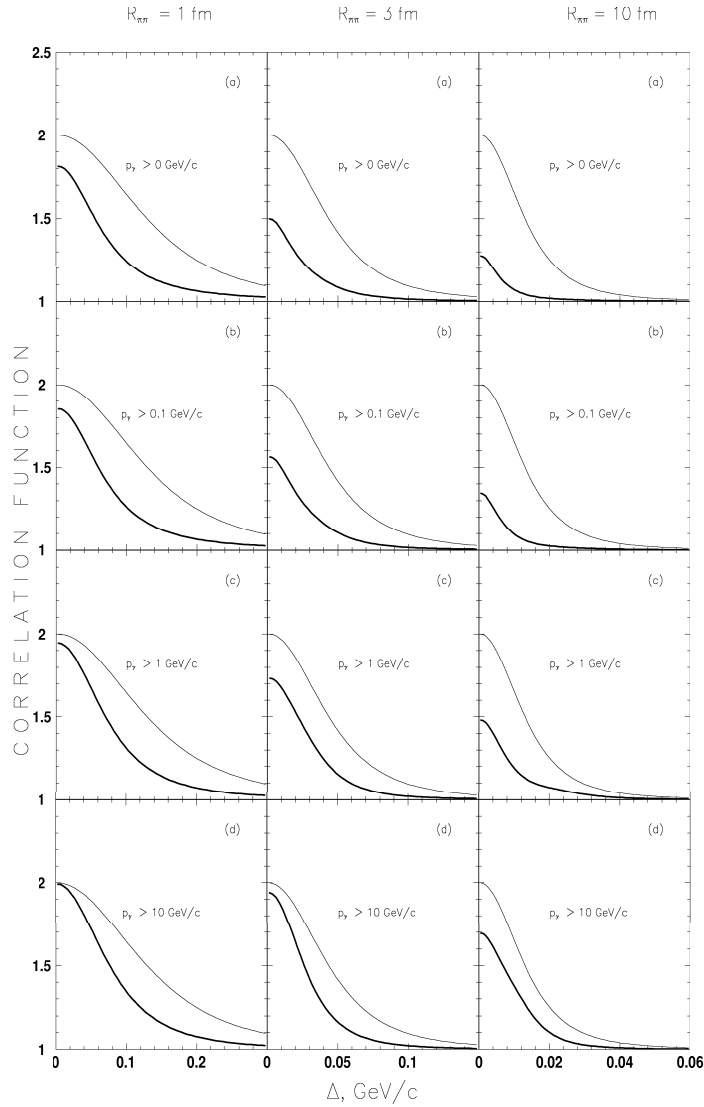


Figure 5.27: $\pi^0\pi^0$ (thin curve) and corresponding $\gamma\gamma$ (thick curve) correlation functions versus the appropriate relative momentum. From reference [23]

- the initial $\pi^0 - \pi^0$ Bose-Einstein correlation is also present in $\gamma\gamma$ pairs and source parameters can be extracted
- the extracted source parameters are related to the original source parameters by a photon momentum dependent function.

Direct photons

As we have learned so far, direct photons have various origins with rather different source's parameters. For simplicity we shall distinguish two sources only: an early one in which photons are produced in the initial parton cascade leading to thermalization of a quark-gluon plasma and a later one where photons are radiated from thermalized matter the quark-gluon plasma phase, the mixed phase or the hadronic phase. Within this photon production dynamic the two-photon correlation function is an unique tool to evidence the early perturbative QCD phase. Indeed the early emitted photons are Bose-Einstein correlated over a wide longitudinal momentum scales, thanks to their very early emission time:

$$\Delta\tau = 0.5 \text{ fm}/c \Rightarrow \Delta p = 0.4 \text{ GeV}/c$$

All other photons that emerge later are correlated at progressively narrower longitudinal momentum scales, which provides a possibility to distinguish the contribution of the early photons and to verify the existence of the hypothetical rapidly developing parton cascade. This is illustrated by two simulations.

- The first one [25] was performed at RHIC energies for the system Au+Au at 200A GeV. The first stage of the collision is calculated within the Parton Cascade Model (see section 3.1). Equilibrium is reached after about 2 fm/c and with a temperature of 950 MeV. The evolution of the equilibrated phase is described by a three dimensional hydro-dynamical model. The direct photon spectrum (no decay photons) from the various phases of the collision (Figure 5.28) indicate that within these calculations (is it realistic?) that pre-equilibrium photons out shine all others contributions (!) already at photon momenta above 1.5 GeV. The correlation function are calculated (Equation 5.8) as a function of the relative rapidity, i.e., in longitudinal direction and relative transverse momentum (Figure 5.29) and for various transverse momentum cuts.. One observes that the shape of the correlation functions changes dramatically when the photon momentum increases and reflects nothing else than the increasing contribution of pre-equilibrium photons. The larger correlation width indicating a narrower source volume and shorter emission time.
- A second calculation [26] was performed for LHC energies. Again the photon production dynamics is separated into two components: early photons emerging at time 0.3 fm/c from the rapidly developing parton cascade at 750 MeV effective temperature and the late photons comprising the later direct photons and the decay photons. It is further assumed that the fraction of the early direct photons is 5% or the total photon yield (Figure 5.30). The two-photon correlation function as a function of the relative longitudinal momentum (Figure 5.31) has been simulated with the longitudinal effective length of 0.3 fm, which corresponds to the early appearance of the hypothetical high effective temperature parton gas. The transverse effective radius was set to 3 fm which corresponds to the transverse size of the colliding Pb nuclei. Gaussian shape has been assumed in the three dimensions with an intercept of 1.5. The expected wide HBT correlation in Q_L (Figure 5.31) due to early photons is indeed seen.

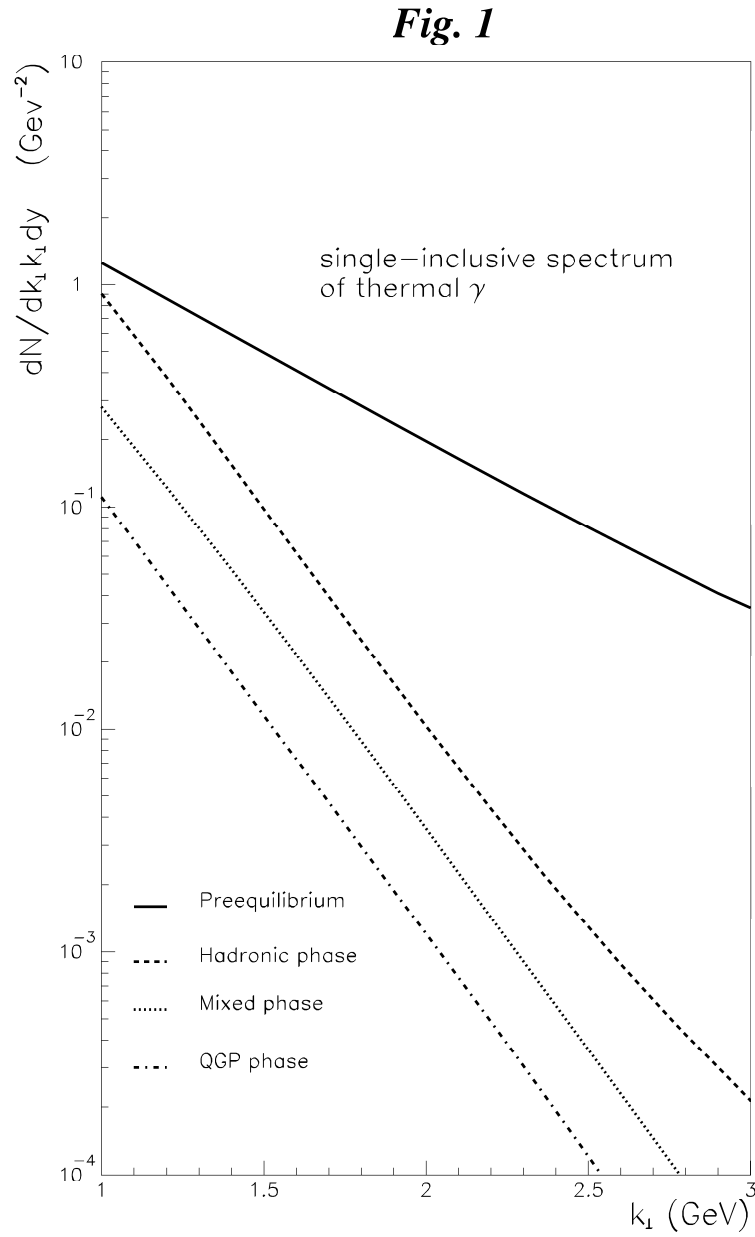


Figure 5.28: Inclusive spectrum of pre-equilibrium and thermal photons for Au+Au collisions at 200A GeV as a function of transverse momentum at $y=0$. From reference [25]

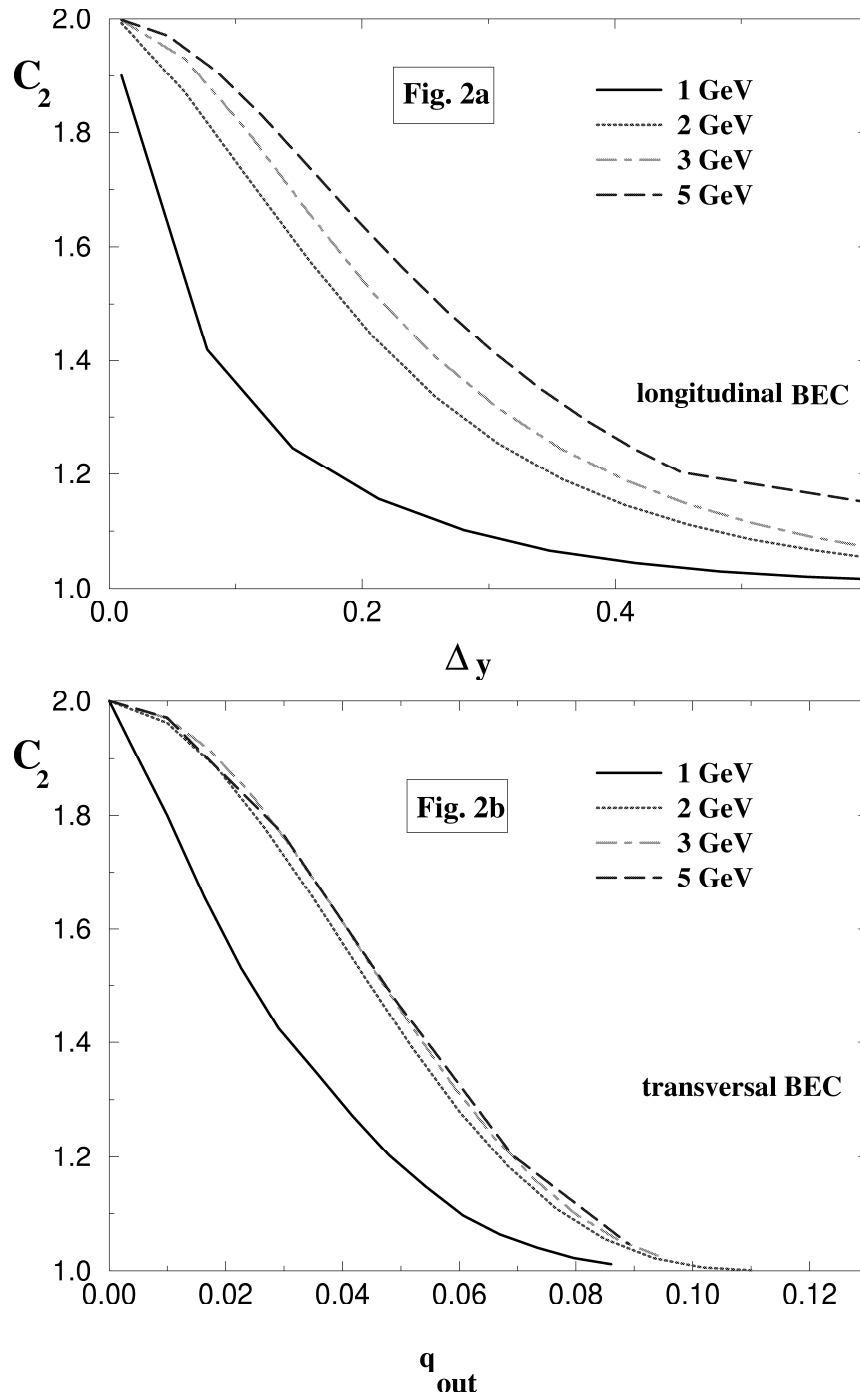


Figure 5.29: Correlation functions of photon as a function of the rapidity difference and the relative transverse momentum calculated for different transverse momenta of one photon. From reference [25].

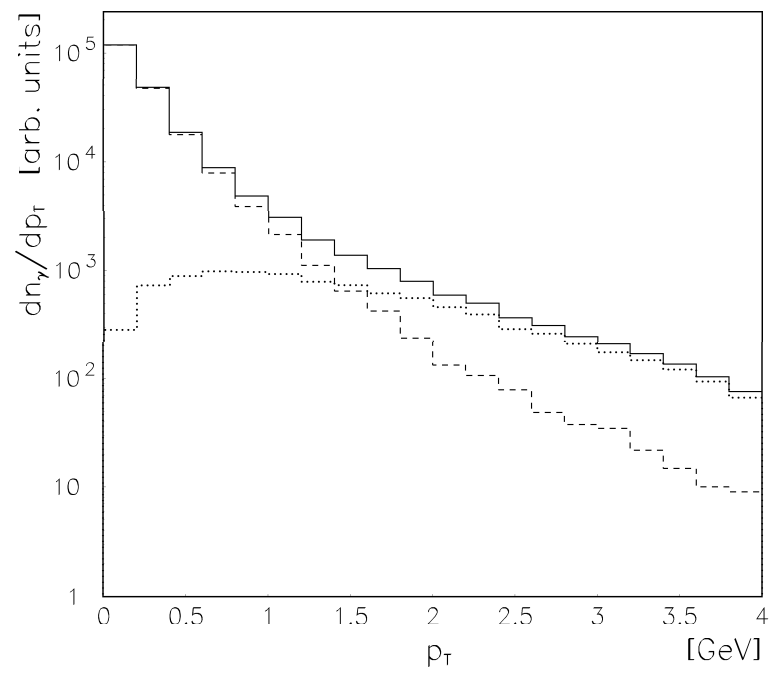


Figure 5.30: Transverse momentum spectra for pre-equilibrium photons (dotted line) and thermal photons (dashed line) and the sum of the two (full line). From reference [26]

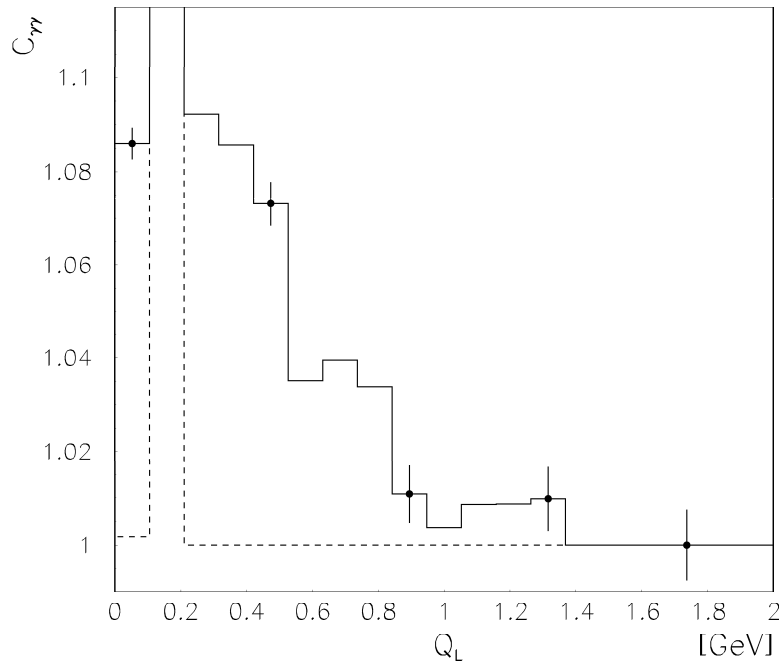


Figure 5.31: Two-photon correlation function as a function of the longitudinal relative momentum with a transverse momentum cut at 2 GeV and $Q_S < 0.1$ GeV, $Q_O < 0.1$ GeV. Full line: $R_L = 0.3$ fm, $R_S = R_O = 3$ fm. Dashed line: the early photon component is shifted to later times by setting $R_L = 6$ fm. The sharp peak is due to the π^0 decay. From reference [26].

As a general conclusion one can say if during heavy-ion collisions a parton cascade phase takes place, it should be seen in the two-photon correlation function along the longitudinal dimension on a wide scale well beyond the π^0 correlation peak and only for large momentum photons.

5.5 Photons and DCC

5.6 Photons and heavy mesons

5.7 Measuring photons

Real photons are notoriously hard to measure. However the instrumental and physics backgrounds are broad. The errors on the measured cross-sections are predominantly the result of systematics errors. The experimental challenges differ if one wants to measure high transverse mass photons or low transverse mass photons.

5.7.1 High momenta photons

High p_t means a few GeV/c.

- The first difficulty comes from necessity to resolve the two photons from the π^0 decay which showers might merge in the detector and appear as a single photon.

$p_t^{\pi^0}$ (GeV/c)	$d_{min}^{\gamma\gamma}$ (cm)	
	PHENIX ($R_{vertex} = 510$ cm)	ALICE ($R_{vertex} = 460$ cm)
20	6.89	6.21
40	3.44	3.10

The solution to that problem is to chose an adequate granularity of the detector: the EMCAL of PHENIX has 5.5×5.5 cm² and 4.0×4.0 cm² and PHOS in ALICE has 2.2×2.2 cm². The next step is to apply a shower shape analysis which is based on the lateral distribution of the electromagnetic shower (Figure 5.32):

$$\begin{aligned}
 f(e, E) &= A \exp\left(-\frac{r^4}{2.32}\right) & r \leq 0.5 \\
 &= A \max\left\{\exp\left(-\frac{r^4}{2.32}\right), d \exp\left(-\frac{r^{0.6}}{s}\right)\right\} & r > 0.5
 \end{aligned}$$

with $d = 1.97$ and $s = 0.385$, A is a normalization factor.

- The low count rates is another problem as shown in the next table taken from reference [7]:

RHIC: $\sqrt{s} = 200$ MeV, Au+Au $\mathcal{L} = 2 \times 10^{26}$ cm ⁻² s ⁻¹				
E_t^γ (GeV)	7	10	15	20
$dN^{\gamma-jet}/dydE_t year$	20500	3550	400	70
LHC: $\sqrt{s} = 5.5$ TeV, Au+Au $\mathcal{L} = 2 \times 10^{27}$ cm ⁻² s ⁻¹				
E_t^γ (GeV)	40	50	60	
$dN^{\gamma-jet}/dydE_t year$	2880	1070	490	

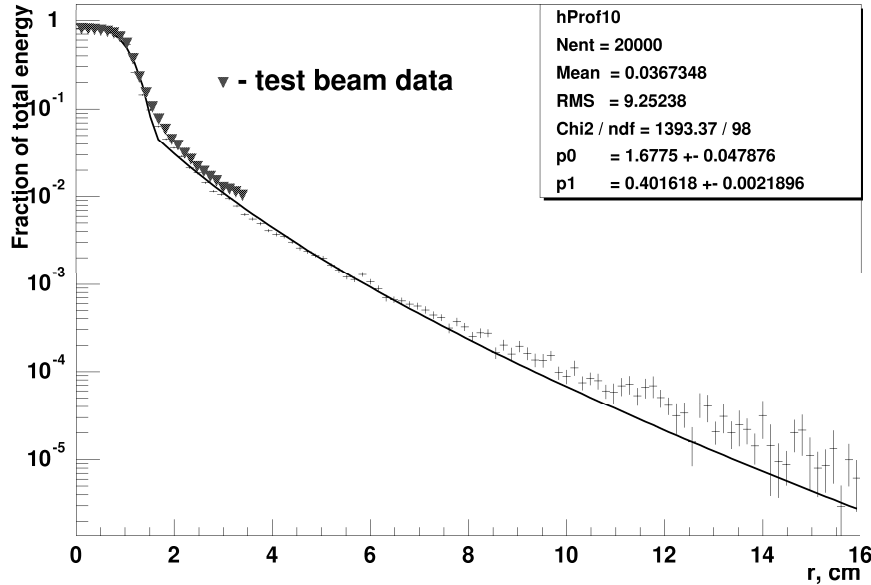


Figure 5.32: Response in one PHOS module relative to the total energy deposit versus the distance to the incident point of a 10 GeV photon.

One therefore requires back-to-back coverage, trigger on high momentum photon/jets and a systematic study of pp, pA and AA.

5.7.2 Low momenta photons

Low p_t means below a few GeV/c.

- The major problem comes from the decay photons of mesons which are about 10 to 100 times more abundant than direct photons (Figure ??).
- In addition the important particle density of the order of $dN/dy \sim 1500$ at RHIC and 8000 at LHC generate a huge combinatorial background as it goes as $(dN/dy)^2$.
- The granularity of the detector (defined by the crystal size, the distance to the vertex and crystal's Moliere radius) is therefore the major parameter and determines the occupancy.
- Particle identification is also an important factor provided by a Charged Particle Veto (PHENIX and PHOS) for charged hadrons, time of flight measurement for neutral baryons (PHENIX) and shower topology analysis for neutral baryons (PHENIX and PHOS).

5.7.3 Extraction of meson spectra

The exact knowledge of the π^0 spectrum is an unavoidable prerequisite of a direct photon measurement. Four methods have been proposed to measure this spectrum.

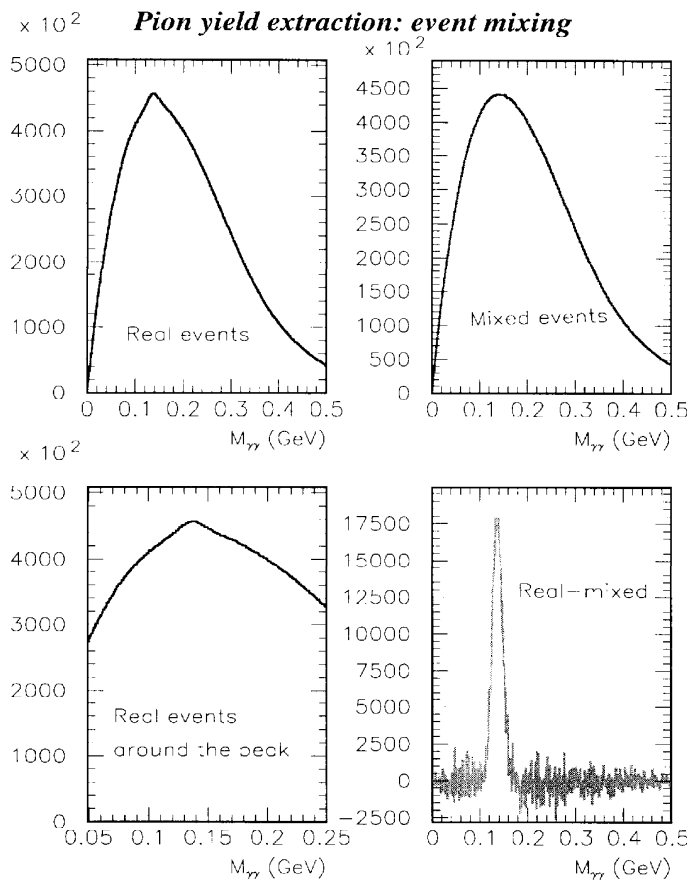


Figure 5.33: Illustration of what an invariant mass spectrum of pairs of photons and the associated combinatorial background will look like . From reference [14]

1. π^0 are identified in the invariant mass spectrum constructed from any pair of photons:

$$M_{inv} = \sqrt{2E_1 E_2 (1 - \cos \theta)}$$

The next step consists in the construction of the combinatorial background to be subtracted from the raw invariant mass spectrum. This background turns out to be a varying function of the transverse momentum and rapidity of the original meson. The most commonly used method to determine the background is the event mixing method. It is generated by constructing the invariant mass between the photons from the current event with each of the photons belonging to an ensemble of different events. The events are classified according to the particle multiplicity. Only events belonging to a same ensemble are mixed.

For those pairs which have their invariant mass around the rest mass of π^0 the 4-momentum of the π^0 can be calculated according to three methods:

- (a) without taking into account the response function of the detector

$$P_\pi = P_{\gamma_1} + P_{\gamma_2}$$

- (b) taking into account the response through the asymmetry of the photon energies:

$$\begin{aligned} \alpha &= \frac{E_{\gamma_1} - E_{\gamma_2}}{E_{\gamma_1} + E_{\gamma_2}} \\ K_\pi &= \sqrt{\frac{2m_\pi^2}{(1 - \cos \phi)(1 - \alpha^2)}} - m_\pi \\ \cos \theta_\pi &= \frac{E_{\gamma_1} \cos \theta_{\gamma_1} + E_{\gamma_2} \cos \theta_{\gamma_2}}{\sqrt{E_{\gamma_1}^2 - E_{\gamma_2}^2 + 2E_{\gamma_1} E_{\gamma_2} \cos \phi}} \end{aligned} \quad (5.10)$$

- (c) the exact solution obtained by minimizing under constraint a function of 12 parameters:

$$\mathcal{F}(E_\pi, \vec{p}_\pi, E_{\gamma_1}, \vec{p}_{\gamma_1}, E_{\gamma_2}, \vec{p}_{\gamma_2}) < \epsilon$$

with the constraints:

$$\begin{aligned} P_\pi &= P_{\gamma_1} + P_{\gamma_2} \\ E_{\gamma_1} &= P_{\gamma_1} \\ E_{\gamma_2} &= P_{\gamma_2} \\ E_\pi &= \sqrt{P_\pi^2 + m_\pi^2} \end{aligned}$$

2. It is considered that the daughter photon spectrum is an integral over all parent π^0 that contribute to a given photon momentum [27]:

$$n(q) = \frac{m_{\pi^0}}{2q^*} \int_{p_{min}}^{p_{max}} \frac{N(p) dp}{(m_{\pi^0}^2 + p^2)^{1/2}}$$

with q, q^* the photon momentum in the laboratory and in the center-of-mass and p the pion momentum in the laboratory. Inverting this equation gives the π^0 spectrum $N(p)$ expressed with the measured single photon spectrum $n(q)$:

$$N(p) = - \left[q \frac{dn(q)}{dq} \right]_{q=\frac{1}{2} [p + (m_{\pi^0}^2 + p^2)^{1/2}]}$$

This method assumes a smooth rapidity distribution for pions and that the inclusive photon spectrum is dominated by the decay photon contribution.

3. A somewhat similar method to the previous one: $g(y, p_t)$ is the measured inclusive photon distribution. Beforehand one needs to construct the transformation matrix $D(y^\gamma, p_t^\gamma : y^\pi, p_t^\pi)$ which relates the single photon inclusive spectrum to the initial parent π^0 distribution. This matrix is purely based on decay kinematics and does not require the *a priori* knowledge of the real π^0 distribution. One then assumes a shape for the π^0 distribution:

$$f(y^\pi, p_t^\pi) = A \exp \left[\frac{(y^\pi - y_0^\pi)^2}{\sigma^2} \right] \exp \left[-m_t^\pi (a + by^\pi + cy^{\pi^2}) \right]$$

and fit the data:

$$g(y^\gamma, p_t^\gamma) = D(y^\gamma, p_t^\gamma : y^\pi, p_t^\pi) f(y^\pi, p_t^\pi)$$

4. The last method [28] compares peripheral and central exclusive spectra. The starting point is that the ratio between peripheral and central particle production cross-sections is the same for all particle species:

$$\frac{\sigma_{peripheral}^{\pi^+}}{\sigma_{peripheral}^{\pi^-}} = \frac{\sigma_{peripheral}^{\pi^0}}{\sigma_{peripheral}^{\pi^0}} \equiv f(p) = \frac{\sigma_{peripheral}^{\gamma hadron}}{\sigma_{peripheral}^{\gamma hadron}}$$

Therefore one can write the inclusive photon spectra in central and peripheral collisions as a sum of direct and hadronic contributions:

$$\begin{aligned} \sigma_{central}^\gamma &= \sigma_{central}^{\gamma direct} + \sigma_{central}^{\gamma hadron} \\ &= \sigma_{central}^{\gamma direct} + f(p) \sigma_{peripheral}^{\gamma hadron} \\ \sigma_{peripheral}^\gamma &= \sigma_{peripheral}^{\gamma direct} + \sigma_{peripheral}^{\gamma hadron} \end{aligned}$$

By subtracting central from peripheral spectra one obtains the direct photon excess:

$$\sigma_{central}^\gamma - f(p) \sigma_{peripheral}^\gamma = \sigma_{central}^{\gamma direct} - f(p) \sigma_{peripheral}^{\gamma direct}$$

No conclusion can, however be obtained on the shape of the direct photon spectrum.

Simulations have been performed to evaluate the capabilities of the event mixing method in the ALICE experiment multiplicity environment. Photons were detected with PHOS, the Photon Spectrometer [29] for ALICE. The SHAKER event generator with highest rapidity density expected in central Pb-Pb collisions, i.e., 8000 charged particles per unit rapidity, has been used to produce π^0 's and η 's. The real and mixed two-photon invariant mass spectra were obtained with and without a cut on α (Equation 5.10). The ratios real/mixed in a p_t range of 2-3 GeV/c for the two cases are shown in Figure

5.7.4 Two-photon correlation function

First a few useful things to remember:

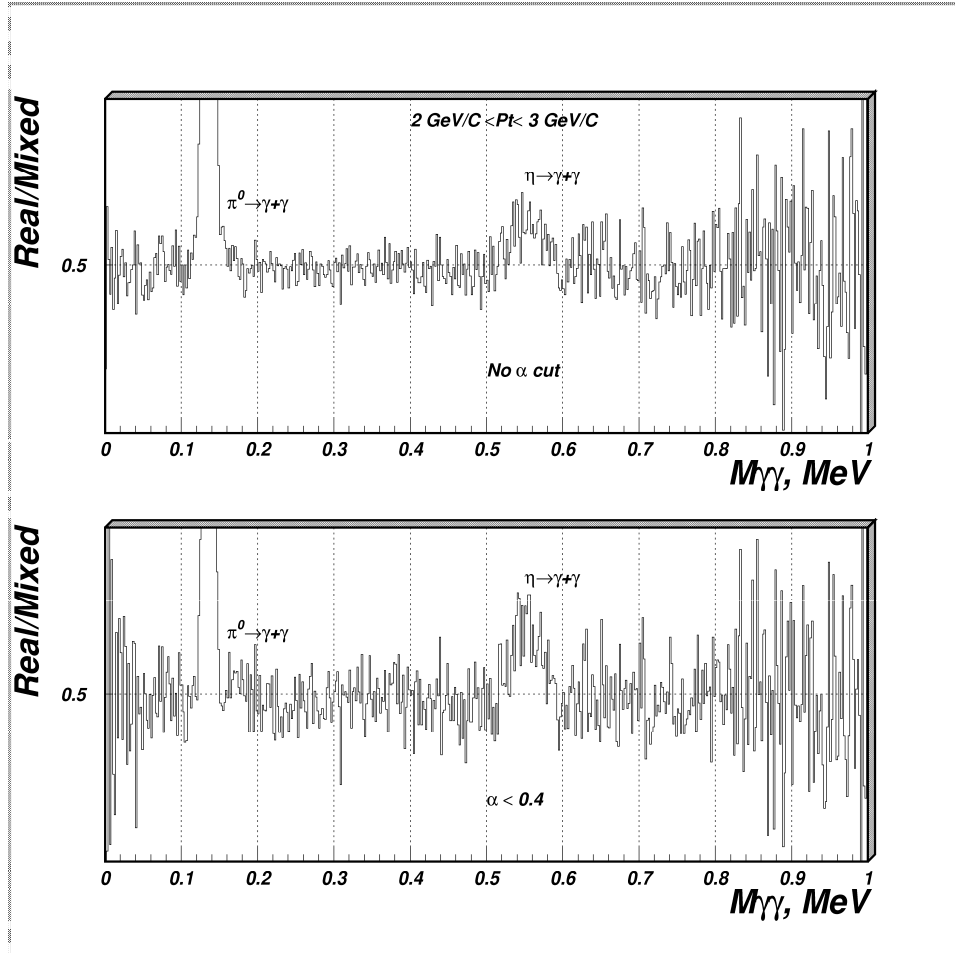


Figure 5.34: Extraction of π^0 and η signals with the event mixing technique and using two cuts in the asymmetry factor (Equation 5.10) of the two photons energy.

- the correlation with when measure in terms of relative momentum Q is related to a spatial extend of the photon production source:

$$R \sim \frac{\hbar c}{Q} \sim 200 \frac{fm \cdot MeV}{Q}$$

and

$$R_{RMS} = \sqrt{\frac{3}{2}} R$$

- The correlation strength for photons is reduced as compared to the strength for hadrons because of the polarization of photons:

$$\lambda = 0.5$$

- The correlation strength is further reduced because of the presence of decay photons:

$$\lambda_{measured} = \lambda_{theory} \left(\frac{N_{\gamma}^{direct}}{N_{\gamma}^{total}} \right)^2$$

i.e., if $N_{\gamma}^{direct}=50\%$, $\lambda = 0.10$ and if $N_{\gamma}^{direct}=10\%$, $\lambda = 0.005$.

The momentum scale along which the two-photon correlation can be measured with PHOS has been evaluated by calculating the two-dimensional acceptance $(\Delta\theta, Q_L)$ (Figure 5.35) for photons with transverse momentum distributed according an exponential distribution with an inverse slope of 500 MeV, $\Delta\theta$ being the opening angle of the two photons and Q_L their relative longitudinal (along the beam axis) momentum. Remember that PHOS maximum opening angle is 30° and the rapidity coverage around mid-rapidity is ± 0.25 . Referring to Figures 5.29 and 5.31 one concludes that the coverage of PHOS will allow to search for the most energetic photons the broad correlation signal expected from pre-equilibrium photons.

5.8 Data and Calculations

The direct photon spectrum has been measured[30] by the WA80 collaboration for 200A GeV S+Au collisions. The calculation are from an hydrodynamic model as described earlier (section 3.2). The various equations of state considered are:

- EOS A (hard) and EOS B (soft) are two different parametrizations (parameters B and K) of an equation of state with a QGP phase transition.
- EOS H is the equation of state for an interacting hadron+resonance gas without phase transition
- EOS I is the equation of state for massless non-interacting hadrons and no phase transition.

Discussion: Depending on the EOS the relative rate of photons from the QGP to the rate from the hadron gas changes:

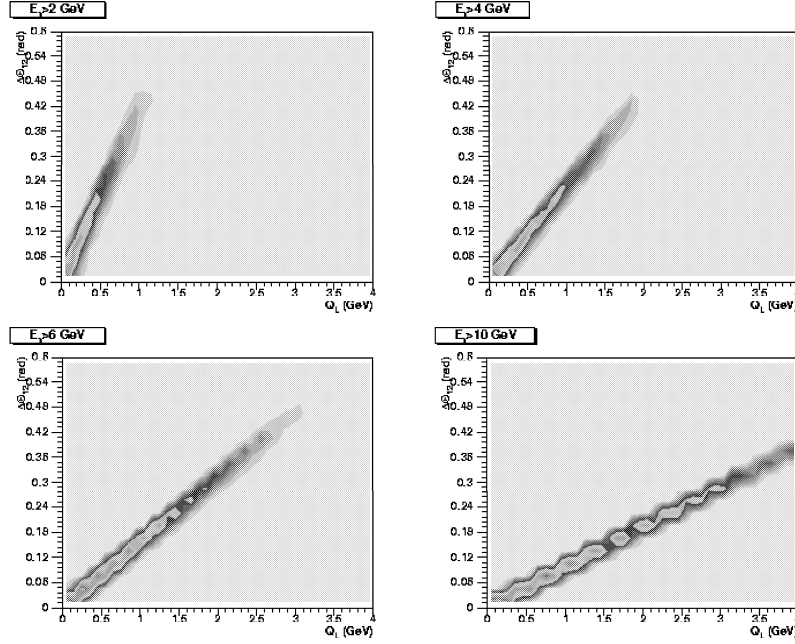


Figure 5.35: Longitudinal momentum scale accessible with PHOS for the two-photon correlation function. It has been calculated for a thermal distribution of photons with $T=500$ MeV.

- QGP leads to larger slope
- Hadron gas leads to a dominant contribution but the QGP contribution can take over at large transverse momentum $p_t \geq 2$ GeV.

In principle the dependence of the photon production on T_C could be used to determine the critical temperature from the data.

EOS	T_0 (MeV)
A	238
B	249
H	248
I	400

Table 5.1: Initial temperatures at t_0 and $z = 0$ calculated for the various EOS of the hydrodynamic model. From reference [4]

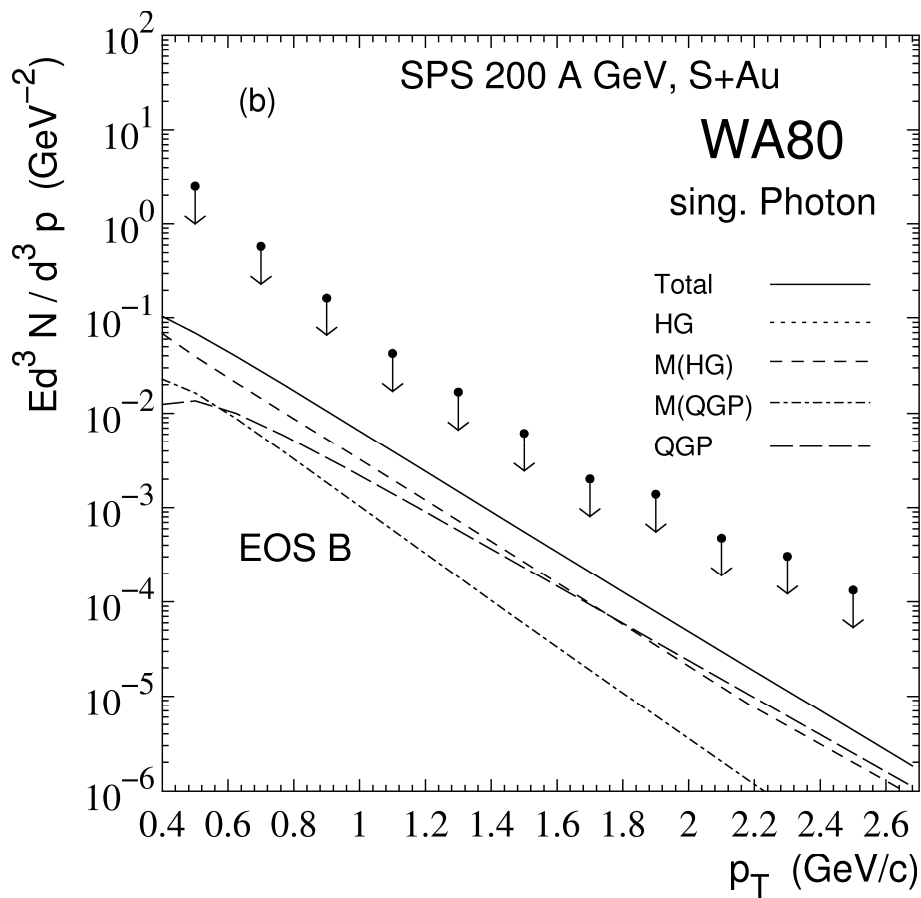


Figure 5.36: Single photon p_T spectra compared with the upper bound of WA80. An EOS with a QGP phase transition is considered and the different contributions are shown: HG hadron gas, $m(\text{HG})$ hadronic part of the mixed phase, $M(\text{QGP})$ QGP part of the mixed phase, QGP quark-gluon plasma phase. From reference [4]

Figure 7b

nucl-th/9607029 16 Jul 1996

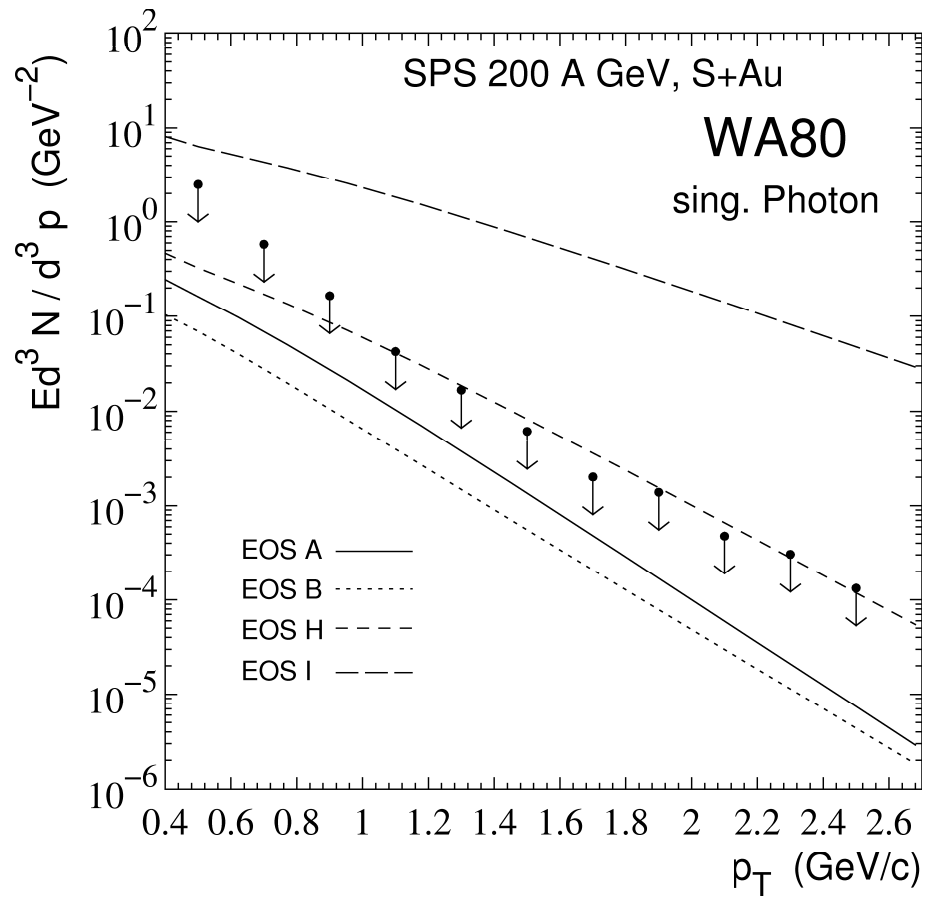


Figure 5.37: Total spectrum of single photons for the different EOS's. From reference [4].

Figure 8

Bibliography

- [1] C.-Y. Wong, *Introduction to High-Energy Heavy-ion Collisions*, World Scientific
- [2] J. Alam, S. Raha, and B. Sinha, *Electromagnetic probes of quark gluon plasma*, Phys. Rep. 273 (1996), 243.
- [3] K. Geiger and B. Muller, *Parton cascade in highly relativistic nuclear collisions*, Nucl. Phys. A544, (1992), 467c.
- [4] J. Sollfrank et al., *Hydro-dynamical description of 200A GeV/c S+Au collisions: Hadron and electromagnetic spectra*, Phys. Rev. C55, (1997), 55.
- [5] D.K. Srivastava, M.G. Mustafa, and B. Müller, *Expanding quark-gluon plasma: Transverse flow, chemical equilibration, and electromagnetic radiation*, Phys. Rev. C56, (1997), 1064.
- [6] X.-N. Wang and M. Gyulassy, *Hijing: a Monte-Carlo program for parton and particle production in high energy hadronic and nuclear collisions*, Phys. Rev. D44, (1991), 3501.
- [7] Xin-Nian Wang, *Effects of jet quenching on high p_T hadron spectra in high-energy nuclear collisions*, hep-ph/9804357 v3 (1998).
- [8] Xin-Nian Wang and Zheng Hung, *Medium-induced parton energy loss in γ +jet events of heavy-ion collisions*, Phys. Rev. C55, (1997), 3047.
- [9] M. Strickland, Phys. Lett. B331, (1994), 245.
- [10] J. Kapusta, P. Lichard, and D. Seibert, *High energy photons from quark-gluon plasma versus hot hadronic gas*, Phys. Rev. D44, (1991), 2774; *Erratum*, ibid D47, (1991), 4171;
- [11] R. Baier, H. Nakkagawa, A. Niegawa, and K. Redlich, *Production rate of hard thermal photons and screening of quark mass singularity*, Z. Phys. C53, (1992), 433.
- [12] P. Aurenche, F. Gelis, R. Kobes, and H. Zaraket, *Two loop Compton and annihilation processes in thermal QCD*, hep-ph/9903307.
- [13] D.K. Srivastava, *Photon Production in Relativistic Heavy-Ion Collisions*, nucl-th/9904010
- [14] EMCAL at PHENIX web pages ([http://http://www.phenix.bnl.gov/](http://www.phenix.bnl.gov/))
- [15] E. Shuryak and L. Xiong, *Dilepton and photon production in the "hot-gluon" scenario*, Phys. Rev. Lett. 70, (1993), 2241.

- [16] A. Dumitru and N. Hammon, *Effect of quark-jet energy loss on direct photons in ultra-relativistic heavy-ion collisions*, hep-ph/9807260 (1998).
- [17] S. Sarkar et al., *Large mass diphotons from relativistic heavy ion collisions*, nucl-th/9704006, (1997)
- [18] J.L. Kapusta, *Photons and lepton pairs from high energy nuclear collisions*, Nucl. Phys. A566, (1994), 45c.
- [19] L. Xiong, E. Shuryak, and G.E. Brown, *Photon production through A_1 resonance in high-energy heavy-ion collisions*, Phys. Rev. D46, (1992), 3798.
- [20] *Optique quantique* in Encyclopaedia Universalis, France 1968, 13-871.
- [21] R.J. Glauber, *Quantum theory of coherence in quantum optics* ed. S.M. Hay & A. Maitland, London, 1970.
- [22] K. Steffens, *Untersuchungen zur korrelierten Produktion von Photonen und neutralen Pionen in Schwerionenreaktionen bei 200A GeV Projektilenergie*, Dissertation, Münster, 1994.
- [23] A. Deloff and T. Siemiarczuk, *Bose-Einstein correlation in a $\pi^0 - \pi^0$ system*, ALICE/98-50 Internal note (1998).
- [24] A. Timmermann, M. Plumer, L. Razumov, R.M. Weiner, *Photon interferometry of quark-gluon dynamics revisited*, Phys. Rev. C50 (1994), 3060.
- [25] U. Ornik, M. Plumer, A. Timmermann, R. W. Weiner, *Pre-equilibrium stage and phase transition of quark matter probed by photon interferometry*, hep-ph/9509367, submitted to Phys. Rev. Lett.
- [26] D. Ferenc, *How to test the existence of the early parton cascade using photon HBT correlations?*, 2nd Catania Relativistic Ion Studies : CRIS '98 Acicastello, Italy ; 8 - 12 Jun 1998.
- [27] G.I. Kopylov, Nucl. Phys. B52, (1973), 126.
- [28] N.J.A.M van Eijndhoven, *On the observability of direct photons in ultra-relativistic nucleus-nucleus collisions by means of inclusive photon and hadron spectra*, I have a draft.
- [29] *Photon Spectrometer PHOS*, CERN/LHCC 99-4, ALICE TDR 2, 5 March 1999.
- [30] R. Albrecht et al., WA80 Collaboration, Phys. Rev. Lett. 76, (1996), 3506.